UNIVERSITY OF LEEDS

This is a repository copy of *The Impact of Fine-scale Reservoir Geometries on Streamline Flow Patterns in Submarine Lobe Deposits Using Outcrop Analogues from the Karoo Basin*.

White Rose Research Online URL for this paper:
http://eprints.whiterose.ac.uk/101844/

Version: Accepted Version

Article:

Hofstra, M, Pontén, ASM, Peakall, J et al. (3 more authors) (2017) The Impact of Fine-scale Reservoir Geometries on Streamline Flow Patterns in Submarine Lobe Deposits Using Outcrop Analogues from the Karoo Basin. Petroleum Geoscience, 23 (2). pp. 159-176. ISSN 1354-0793

https://doi.org/10.1144/petgeo2016-087

© 2016 The Author(s). Published by The Geological Society of London for GSL and EAGE. This is an author produced version of a paper published in Petroleum Geoscience. Uploaded in accordance with the publisher's self-archiving policy.

Reuse

Unless indicated otherwise, fulltext items are protected by copyright with all rights reserved. The copyright exception in section 29 of the Copyright, Designs and Patents Act 1988 allows the making of a single copy solely for the purpose of non-commercial research or private study within the limits of fair dealing. The publisher or other rights-holder may allow further reproduction and re-use of this version - refer to the White Rose Research Online record for this item. Where records identify the publisher as the copyright holder, users can verify any specific terms of use on the publisher's website.

Takedown

If you consider content in White Rose Research Online to be in breach of UK law, please notify us by emailing eprints@whiterose.ac.uk including the URL of the record and the reason for the withdrawal request.

White Rose
university consortium
Universities of Leeds, Sheffield & York

eprints@whiterose.ac.uk
https://eprints.whiterose.ac.uk/

The Impact of Fine-scale Reservoir Geometries on Streamline Flow Patterns in Submarine Lobe Deposits Using Outcrop Analogues from the Karoo Basin

M. Hofstra[a]*, A.S.M. Pontén[b], J. Peakall[a], S.S. Flint[c], K.N. Nair[b], & D.M. Hodgson[a]

[a] Stratigraphy Group, School of Earth and Environment, University of Leeds, Leeds, LS2 9JT, UK

[b] Statoil ASA, Research Centre Rotvoll, NO-7005 Trondheim, Norway

[c] Stratigraphy Group, School of Earth, Atmospheric and Environmental Sciences, University of Manchester, Manchester M13 9PL, UK

** Correspondence (eemh@leeds.ac.uk)*

Running Header: Fine-scale Reservoir Modelling of Lobes

ABSTRACT: Improved prediction of the recovery of oil-in-place in basin-floor fan reservoirs requires accurate characterisation and modelling of multiscale heterogeneities. The use of outcrop analogues is a key tool to augment this process by documenting and quantifying sedimentary architecture, hierarchy, and sedimentary facies relationships. A 3D geological modelling workflow is presented that tests the impact of fine-scale heterogeneities within basin-floor lobe complexes on reservoir connectivity. Construction of geological models of a basin-floor lobe complex allows realistic depositional architecture and facies distributions to be captured. Additionally, detailed models are constructed from channelised areas within a basin-floor lobe complex. Petrophysical modelling and streamline analysis are employed to test the impact on reservoir connectivity between lobe models with i) vertically-stacked facies with coarsening- and thickening-upwards trends in all locations, and ii) lateral facies changes with dimensions and distributions constrained from outcrop data. The findings show that differences in facies architecture, and in particular lobe-on-lobe amalgamation, have a significant impact on connectivity and macroscopic sweep efficiency, which influence the production results. Channelised lobe areas are less predictable reservoir targets due to uncertainties associated with channel-fill heterogeneities. The use of deterministic sedimentary architecture concepts and facies relationships have proven vital in the accurate modelling of reservoir heterogeneities.

Keywords: Fine-scale reservoir modelling; Reservoir connectivity; Sweep efficiency; Streamline simulations; Submarine lobes; CLTZ; Karoo Basin

INTRODUCTION

Hydrocarbon production targets are moving towards more challenging reservoir types, including offshore turbidite reservoirs in ultra-deep settings. Typically, the construction of geological models for these reservoirs uses a combination of subsurface seismic and well data. Well data is particularly sparse during the early phase of projects (Strebelle *et al.* 2003; Pyrcz & Deutch 2014) and seismic resolution is inadequate to constrain 3D reservoir connectivity and heterogeneity distribution. Therefore, outcrop analogues and conceptual models are applied to reduce this uncertainty (e.g. Bryant & Flint 1993; Pringle *et al.* 2006; Howell *et al.* 2014).

Application of outcrop data helps to capture architectural complexity and heterogeneities within submarine fan (sheet) systems (e.g. Kleverlaan & Cossey 1993; Richards & Bowman 1998; Drinkwater & Pickering 2001) and to constrain stochastic-based modelling of facies and petrophysical properties (Alabert & Massonnat 1990; Joseph *et al.* 2000; Stephen *et al.* 2001; Amy *et al.* 2013). A small number of studies have performed stochastic-based modelling of submarine lobe deposits, where individual compensationally stacked flow events were modelled to create lobate geometries or sheet-like splays (Pyrcz *et al.* 2005; Saller *et al.* 2008; Zhang *et al.* 2009). Recent work (e.g. Pirmez *et al.* 2000; Beaubouef *et al.* 2003; Deptuck *et al.* 2008; Prélat *et al.* 2009, 2010; Macdonald *et al.* 2011; Straub & Pyles 2012) has demonstrated that submarine lobe architecture and facies trends are often not as simple as the classical models (e.g. Mutti *et al*. 1977; Mutti & Sonnino 1981), and involve stratigraphic order and hierarchy (Prélat *et al.*, 2009; Straub & Pyles, 2012), which may not be covered within purely stochastic modelling methods. The planform extent of submarine lobes in the subsurface can be resolved by seismic mapping (Saller *et al.* 2008), however smaller-scale elements and heterogeneities cannot be seismically resolved. Attributes (Fig. 1), such as lobe amalgamation and internal facies transitions (e.g. Stephen *et al.* 2001; Zhang *et al.* 2009) have proven to have a major impact on reservoir model predictions, but their relative impact is poorly constrained. Other attributes such as finger-like geometries within lobe fringe areas

(Groenenberg *et al.* 2010) and the juxtaposition of channels and lobes in Channel-Lobe Transition Zone-s (CLTZs), have never been captured in published reservoir modelling work.

The architectural complexity of submarine channel-levee complexes and their influence on reservoir performance (e.g. Clark & Pickering 1996; Stephen *et al.* 2001; Larue 2004; Larue & Friedmann 2005; Sprague *et al.* 2005; Mayall *et al.* 2006; Schwarz & Arnott 2007; Barton *et al.* 2010; Pringle *et al.* 2010; Alpak *et al.* 2013; Labourdette *et al.* 2013; Eschard *et al.* 2014) has been widely studied. The main focus of this work was on the diversity of channel architecture and heterogeneities within channel-fills, such as channel base drapes (e.g. Larue & Friedmann 2005; Barton *et al.* 2010; Alpak *et al.* 2013). Detailed studies on facies characteristics in turbidite reservoirs (e.g. Stephen *et al.* 2001; Falivene *et al.* 2006; Scaglioni *et al.* 2006) demonstrate that heterogeneities across a range of scales influence connectivity and compartmentalisation of the reservoir. Pore and textural properties in structured and normally graded sandstones will affect flow properties of the bed and the system as a whole (Stephen *et al.* 2001). The focus on the presence or absence of large-scale baffles and barriers such as shale drapes (e.g. Stephen *et al.* 2001; Saller *et al.* 2008; Barton *et al.* 2010; Pyrcz & Deutsch 2014) will not capture the whole spectrum of heterogeneities. In contrast to channel-levee complexes, there are only a small number of fine-scale reservoir heterogeneity studies from channel-lobe transition zones, despite being important deep-water reservoir targets. Connectivity of channel-fills with overbank deposits (Eschard *et al.* 2014), and reservoir performance differences between lobe and channel-fill dominated deposits (Zou *et al.* 2012) are poorly understood. Zou *et al.* (2012) noted that sheet-prone sandstones provide more sustained production than channel-prone sandstones due to a significant decrease in sweep efficiency in the latter. Margin connectivity within channel-lobe contacts can be in many cases much better compared to channel-channel or channel-levee contacts (Funk *et al.* 2012).

Here, we aim to study and quantify the impact of different conceptual stratigraphic and sedimentological models of deep-marine lobes on reservoir behaviour and fluid flow predictions, and compare these sedimentological and stratigraphic factors to other uncertainties within reservoir modelling. This aim was addressed through the application of both 'hard' (geometric) and 'soft' (understanding) data (*sensu* Howell *et al.* 2014) from outcrop analogues of exhumed basin-floor lobe and channel-lobe transition zone deposits from the Karoo Basin, South Africa. Soft data includes conceptual models, characteristic facies for architectural elements and their lateral or vertical facies relationships. The objectives of this study are to follow a deterministic modelling approach to investigate the effect of sub-seismic heterogeneities within lobe complex sub-environments (Fig. 1) on reservoir connectivity, including 1) lobe amalgamation, 2) facies transitions and distributions and, 3) channelisation. Sensitivity tests on various petrophysical models are performed with the help of 275 single-phase streamline flow simulations.

METHODS

Outcrop datasets from the Tanqua depocentre were used to construct sedimentary facies grid models (Fig. 2) within a cornerpoint grid mesh using the commercially available software Reservoirstudio^{TM}. The sketch-based interface and cornerpoint grid of the software permits construction of complicated depositional architectures of lobes and channels, including fine-scale vertical heterogeneity with a low amount of total grid cells. Conventional modelling methods using Cartesian grid meshes are unable to capture small-scale heterogeneities as they are limited to the shape and size of the cells (Aarnes *et al.* 2008; Jackson *et al.* 2015).

Separate grid frameworks were used to construct a lobe complex (full lobe-scale models) and two channel-lobe transition zone scenarios (lobe-scale sector models) (Fig.2). Single-phase flow streamline simulations were performed between vertical injector and producer wells, to investigate differences in connectivity and production performance (Fig.2).

Regional setting of outcrop analogues

The Karoo Basin is one of several late Palaeozoic to Mesozoic basins that formed on the southern margin of Gondwana in response to convergent-margin tectonism (De Wit & Ransome 1992; Veevers *et al.* 1994; López-Gamundi & Rosello 1998). The southwestern area of the Karoo Basin is divided into two depocentres: the Tanqua and Laingsburg depocentres (Flint *et al.* 2011). In the Tanqua depocentre (Fig. 3), the upper Ecca Group comprises a shallowing-upwards succession from distal basin-floor mudrocks (Tieberg Formation), through basin-floor fans (Skoorsteenberg Formation) to shelf-edge delta deposits (Waterford Formation). The Late Permian Skoorsteenberg Formation (Fildani *et al.* 2009; McKay *et al.* 2015) is 400 m in thickness and comprises five distinct sand-rich submarine fan systems, which are separated by laterally extensive hemipelagic mudstones (Johnson *et al.* 2001; Van der Werff & Johnson 2003; Hodgson *et al.* 2006). Fan 3 is the most extensively studied system (Bouma & Wickens 1991, 1994; Sullivan *et al.* 2000; Johnson *et al.* 2001; Van der Werff & Johnson 2003; Hodgson *et al.* 2006; Hofstra *et al.* 2015), showing the transition from base-of-slope to distal pinch-out. Prélat *et al.* (2009) and Groenenberg *et al.* (2010) studied the basin-floor lobe deposits within Fan 3 and showed the importance of autogenic processes that drive compensational stacking patterns. Unit 5 represents the transition from a basin floor to slope environment (Van der Werff & Johnson 2003; Wild *et al.* 2005; Hodgson *et al.* 2006), and was fed by multiple channel systems, in contrast to the underlying point sourced fan systems (Hodgson *et al.* 2006).

Outcrop data collection and interpretation

Three study areas were used to build facies model frameworks: a distal basin-floor lobe dataset of Fan 3 (BFL) based on Hodgson *et al.* (2006), Prélat *et al.* (2009) and Prélat (2010), and two newly collected datasets from CLTZ environments, one from Fan 3 and one from Unit 5 (Fig. 3). For reconstructing a full-scale basin-floor lobe complex, the hierarchical scale and sedimentary concepts of Prélat *et al.* (2009) and Prélat & Hodgson (2013) have been followed. These provide a unique data-set from the medial to distal areas (Fig. 3) with closely spaced measured sections across a 150 km^2 study area of Fan 3 with lateral constraints on individual lobes and facies distributions due to good outcrop extent and limited amount of erosion (Fig. 4). Lobe facies maps and lobe thickness information (Prélat *et al.* 2009; Groenenberg *et al.* 2010) underpin the facies modelling of the basin-floor lobe complex.

For the CLTZ models, two segments from base-of-slope channelised lobe areas were chosen and sedimentary log data collected: Ongeluks River (OR) of Fan 3 and Blaukop (BK) in Unit 5 (Fig. 3). These study areas augment previous work (Kirschner & Bouma 2000; Sullivan *et al.* 2000, 2004; Van der Werff & Johnson 2003; Hodgson *et al.* 2006; Luthi *et al.* 2006) and show clear differences in the character of channel-fills and channel volumes and their stratigraphic and physical relationship with underlying lobe deposits.

The OR area preserves a distributive channel network that incises tabular sand-prone packages which have been referred to as 'intra-channel highs' (Van der Werff & Johnson 2003; Sullivan *et al.* 2004; Luthi *et al.* 2006) (Fig. 5). Due to their sandstone-prone nature and variation in bed thicknesses, they are here interpreted as a combination of lobe and overbank deposits. A new dataset was collected with thirty-four measured sections (25-50 m spacing) within a 2 km wide EW-trending section, which form the basis of the OR model framework. The eight channel-fills show a range of cross-sectional geometries (100-550 m wide, 4-10 m deep), and are vertically and laterally stacked with occasional lateral overlap (Fig. 5).

The BLK-section of Unit 5 shows two confined channel systems (~300-350 m wide & >10 m deep) incised into sandstone-rich deposits (Kirschner & Bouma 2000). Twenty-seven sedimentary logs were collected in a 2 km^2 area with close-spacing (10 to 100 m apart), permitting the construction of a 3D framework. In addition, one fully cored borehole (BK01) was drilled 150 m away from the nearest outcrop, allowing bed-to-bed correlation with the outcrop dataset.

Basin floor lobe complex (BFL)

The medial to distal part of the Fan 3 lobe complex consists of six lobes, and facies and thickness maps have been constructed for four of them (Fig. 6). Thin beds between lobes were originally referred to as interlobes (Prélat *et al.* 2009), although Prélat & Hodgson (2013) subsequently interpreted these as the distal fringes of other lobes, due to compensational stacking. Facies models were constructed for a lobe complex including the four lobes (Fig. 6) and at the scale of the model (20 km x 40 km x 70 m) the interlobes were treated as through-going fine-grained units. Due to this rectangular mesh framework (20 km x 40km), rectangular cells were used, 200 m wide (x) and 300 m long (y) and with variable z cell dimensions (0.25 - 20 m). Reservoirstudio^{TM} permits complicated planform architectures of submarine lobes to be drawn and constructed. The scheme of Prélat *et al.* (2009) was applied to define four distinct sub-environments of lobe deposition: axis, off-axis, fringe and distal fringe. This subdivision was also applied within the modelling process; however the fringe and distal fringe were combined to a single 'fringe' sedimentary facies zone. Sedimentary facies associations were attributed to each of the zones within the lobe models, creating realistic facies distributions and vertical stacking patterns. Distinct lobe areas (zones) were created that closely follow the patterns of the original facies distribution (Fig. 6) including lobe fingers (Groenenberg *et al.* 2010). With only three sedimentary facies zones, some simplification of facies modelling was necessary. No distinction was made between frontal and lateral fringes, and hybrid-bed prone areas (Hodgson 2009) were not included. Lobe and interlobe thickness information were implemented in each individual lobe, and adapted for each lobe zone.

Two conceptual models of lobe architecture and facies distribution were tested (Fig. 7): Model A, 'classic' lobe model (coarsening- and thickening-upwards at all locations within the lobe) and Model B, the Karoo-based conceptual lobe model (facies transitions from axis to fringe and allowing lobe amalgamation). The classic model (Model A) (Fig. 7) follows the Marnoso model of Ricci-Lucchi (1975); Mutti (1977); Mutti & Sonnino (1981); Piper & Normark (1983) or the 'Depositional Lobes' model from Shanmugam & Moiola (1991), in which all facies zones are vertically stacked within each lobe. This implies that fringe zones formed the base of each lobe and covered the whole lobe area. The remaining lobe zones show progressively smaller surface areas, mimicking a stratigraphic pattern of coarsening- and thickening-upwards across the entire volume of the lobe, implying an overall progradational pattern (Prélat & Hodgson 2013). The facies-transition model (Model B - Prélat *et al.* 2009) (Fig. 7) shows multiple lateral transitions from axis to fringe areas to capture compensational stacking of lobe elements. The axial lobe areas were made slightly erosional, mimicking lobe amalgamation in axial areas (Prélat *et al.* 2009). Different facies associations have been attributed to each lobe zone based on sedimentary log data. A total of three different facies associations were used for the basin-floor lobe complex models: thick-bedded structureless sandstone (Fa1), medium-bedded structured sandstones (Fa2) and thin-bedded siltstones and sandstones (Fa3).

Within Model A the number of facies groups decreases from axis to fringe, with Fa3 being spread over the complete surface area of the lobe, Fa2 only covering the two inner zones (off-axis and axis) and Fa1 being focused within the axis. All together this resembles a coarsening-upward trend.

For Model B, three sub-models were constructed with different proportions of facies associations for the different lobe zones (Fig. 7). The vertical lobe structure was divided in three packages (top, middle and bottom) of which the middle portion was twice as thick as the top and bottom portions. The three sub-models represent three different levels of internal detail with B1 – one facies group for each lobe zone, B2 – multiple facies groups for off-axis and fringe zones, B3 – multiple facies groups for all lobe zones. Due to these differences in facies proportions within the lobe zones, the style of facies transitions that has been modelled from axis to fringe is more abrupt in B1 and B2 than in B3. Attempt was made to keep the overall facies volumes constant between the different BFL models (Fig. 7), to prevent major reservoir performance differences due to variance in overall petrophysical properties.

CLTZ environments (OR & BK)

Small-scale sector models (2 km x 2 km x 70 m) were created for the two CLTZ environments (BLK & OR) (Fig. 8). All non-channel deposits, including lobes, have been modelled as background layering, representing infinite tabular bodies. This is considered to be sufficient due to the minimal lateral changes in thickness or facies documented at the scale of model in the outcrop data collected from the non-channel deposits. Channel-fills within basin-floor settings of the Karoo Basin dominantly comprise well-sorted structureless sandstones (e.g. Sullivan *et al.* 2000; Johnson *et al.* 2001; Van der Werff & Johnson 2003; Brunt *et al.* 2013), and are well exposed at outcrop (Fig. 5A). Areas of poor exposure were interpreted as intra-channel overbank and lobe deposits. Sedimentary thicknesses and facies distributions were based on sedimentary log-data (Figs. 5 & 8). Realistic depositional architectures for the channel bodies were based on a combination of outcrop observations and generalised models of base of slope channels within the Karoo (e.g. Van der Werff & Johnson 2003; Brunt *et al.* 2013). Some of the tabular sandstone-prone deposits within the BK study area, have been interpreted as very high-aspect ratio channel-fills (Kirschner & Bouma 2000). However, due to their uniform thickness over the study area and tabular nature, here they are interpreted as lobes and overbank material and constructed as part of the background layering. Typically, basin-floor channel-fills (200-400 m wide, 5-10 m deep) in the Karoo Basin are comprised of four main facies groups (Brunt *et al.* 2013; Fig. 5B): amalgamated structureless sandstone (Fa1), medium-bedded banded argillaceous or 'dirty' sandstone (Fa5), mudstone clast lag conglomerate (Fa4) and soft-sediment deformed deposits (Fa6). Fa 1 is the dominant facies group (>75%; Fig. 4A). Typically, with a conventional modelling technique using a regular grid, the channel-fill would be represented by a single facies group, as the incorporation of minority facies would lead to an impractically large number of grid cells. However, the heterolithic character of the facies groups can have significant influence on the reservoir properties. Therefore, two versions of the channel-fills were applied: one with a single-facies fill (Fa1), and one with the addition of the minor facies groups (Fa 1A, Fa4, Fa5 & Fa6). Due to the lack of longitudinal constraint on the channel-fills, standard deviations (0.1-0.5 m) were set for the thickness modelling of each individual facies package. In each CLTZ model, the x and y cell dimensions were set to 100m x 100m, while the z cell was variable between 0.1 to 20 m, depending on the scale of the modelled architecture.

Petrophysical properties are likely to be different in thick amalgamated structureless deposits (Fa 1A) and stratified normally graded sandstones (Fa1B), and therefore a distinction is made. The OR dataset (Fig. 8A) was used to construct two alternative sub-models, OR-A and OR-B, with different levels of detail. OR-A represents a simplified (upscaled) facies model, only including the facies groups that represent the majority of the facies (Fa1A, Fa1B, Fa2 & Fa3) and a more detailed and realistic facies model (OR-B) with the addition of Fa4, Fa5 and Fa6 groups. In addition, some of the background packages were separated into smaller facies packages. Within OR-B the sandstone-rich units were separated into structureless, banded and structured sandstones (Fa1B, Fa2 & Fa4) and the sandstone-poor units into thin-bedded siltstones and structured sandstones (Fa2 & Fa3). The total number of grid cells increased by an order of magnitude (from $70x10^3$ in OR-A to $50x10^4$ in OR-B) with the down-scaling from OR-A to OR-B.

Three sub-models were built with the BK-dataset, which were used to understand the influence of channel architecture on reservoir connectivity. The configuration of the background layering was kept constant and consists of a combination of structured sandstones (Fa2), banded sandstones (Fa5) and thin-bedded sandstones and siltstones (Fa3). Two sub-models showed different levels of channel-fill detail: BK-A single facies group for entire channel-fill, and BK-B enhanced channel-fill facies with the addition of Fa4, Fa5 and Fa6. A third sub-model (BK-C) was constructed, where the channel-fills were completely removed and comprised only background layering. In both the OR and BK models, differences within facies proportions of sub-models were minor (Fig. 8).

Petrophysical property modelling

No petrophysical property dataset is directly usable from the outcrop analogues which have been altered due to burial metamorphism and weathering (Fildani *et al.* 2009). Therefore, data were obtained from the Glitne Field, a small oil field within Paleocene turbidites in the upper part of the Heimdal complex in the South Viking Graben, Norwegian North Sea (Keogh *et al.* 2008). Previous authors have used geometrical constrains and facies information from the Tanqua submarine systems as an outcrop analogue for the Glitne system (Hodgetts *et al.* 2004; Keogh *et al.* 2008). Therefore, petrophysical properties and production data from this field were used for fluid modelling purposes of this study.

Core plug permeability measurements were used from the most central exploration well (15/5-5) within the field (Fig. 9A). The well is positioned between two other exploration wells which have been interpreted as a feeder channel (15/5-6) and a lobe fringe environment (15/5-3) (Avseth *et al.* 2001). Well 15/5 represents a setting where both channel and lobe deposits are interpreted. The core plug measurements were assigned to different facies associations by use of core photographs (e.g. Fig. 9A). These data provided a basic understanding of the range in permeability values (1.2-1200 mD/cP) that can be expected from the various facies associations and the assumption is made that these core plug measurements are representative for the proposed facies groups over their complete cell volume (Ringrose & Bentley, 2015). Remaining permeability values (Fa3; Fa4) were based on Amy *et al.* (2013). To account for the heterolithic character of some of the facies groups (horizontal *versus* vertical permeability), Kv/Kh permeability factors were applied to certain facies groups (Fig. 10), primarily based on Amy *et al.* (2013). A permeability factor was applied within the banded sandstone facies group (Fa5) as the Glitne core data indicated low permeabilities within argillaceous intervals (Fig. 9A) (9 mD/cP compared to >200 mD/cP in non-argillaceous sandstones). Commonly, banded sandstones show a clean dewatered sandstone base and an argillaceous top (Hofstra et al., 2015), an estimate of 0.0125 Kv/Kh (10/800) was applied for the banded facies group. Highest permeability readings (1200 mD/cP) within the 15/5 core are associated with dewatered (dish and pillar structures) clean sands (Stow & Johansson 2000). As this value is significantly higher than other structureless sandstone readings (300-600 mD/cP) a division was made between dewatered amalgamated structureless sandstones (Fa1A) and thick-bedded non-dewatered structureless sandstones (Fa1B). For the Fa3 and Fa4 groups, permeability factors (Kh/Kv) have been estimated, as the dominance of normal grading and the interbedding with low-permeable siltstones will result in heterogeneous vertical petrophysical properties (Scaglioni *et al.* 2006).

As porosity data were not available from the Glitne Field, estimations were applied based on the collection of core porosity data from subsurface Tertiary turbidite systems of Bennes & Hamon (2007) (Fig. 9B) and Amy *et al.* (2013). Both ‘permeability-porosity’ and ‘grain size-porosity’ cross-plots were used to determine porosity ranges for each sedimentary facies group (Fig. 9B). The porosity range was based on the spread of data-points present within this study. To account for the uncertainty within petrophysical properties, ranges were set (Fig. 10) and a total of 25 petrophysical property realisations were performed for every submodel within $\text{RMS}^{\text{TM}}_{2012}$ (Fig. 11).

Streamline simulation set-up

To test connectivity within the reservoir models, single-phase flow simulations have been performed (blue fluid/red fluid simulation in industry appellation) using the streamline analysis tool in $\text{RMS}^{\text{TM}}_{2012}$. This simulation tool allows extremely fast analysis of flow patterns within reservoir models, even when the model is complicated and/or large. The main advantage of this method is that a large number of simulations can be run in a short amount of time (e.g. Brandsæter *et al.* 2001). This allows the performance of a large number of sensitivity tests to look at the relative impact of various factors on flow patterns. The visual representation of flow patterns, called streamlines, show the path of fluid particles through a reservoir, given constant pressure and reservoir conditions. Within the streamline simulation procedure, the boundary conditions are defined by the well rates and the structural boundaries. Once the pressure distribution is calculated, the velocity field is determined, which forms the basis for the streamlines. With the help of these streamlines, differences between scenarios in the preferred flow paths can be identified readily. Due to the large number of simulations (275), the tracer breakthrough times (TBT) between injector and producer wells can be used to evaluate the connectivity within the reservoir. A fast tracer breakthrough between injector and producer well is here associated with increased connectivity and/or permeability contrasts (Hovadik & Larue 2007). As the flow of any fluid or gas in a reservoir is primarily controlled by the spatial distribution of permeability and pressure gradients (Hewett, 1986), contrasts in the permeability due to the presence of different lithofacies will impact reservoir connectivity. For a number of scenarios, drainage functions are performed with the help of generated time-of-flight parameters and pore volumes. These drainage functions give predictions of the production rate using calculated pore volume, time of flight parameters and production/injection regions from the streamline simulation output.

Well set-up

In the basin-floor lobe complex (BFL), two injector-producer pairs (Fig. 12) were sited: one in the axis of the complex (Axis) and one in the fringe area (Fringe). Within the OR-models, three injector-producer pairs were placed, longitudinal to the channel orientation (Fig. 12), with injectors and producers penetrating the same channel system (Loc1,Loc2 and Loc3). For the BK-models, one injector-producer pair was placed longitudinal to channel orientation, penetrating both channel systems (Fig. 12). Well positions were kept constant between all simulations.

Dynamic rock, dynamic fluid (light oil) and reference pressure were based on data from the Glitne Field. Fluid injection and production occurred over the complete modelled interval. To assure a steady state was reached within each simulation, sensitivity tests were performed and the solution time was set to 10 years (3650 days). The distance between injector and producer was always set to a minimum 1km to ensure active flow. In some cases, where multiple injector-producer pairs are present within a single model, an injector of one pair may interfere with the results of a producer well of another pair. The effects of different injectors on the producer wells could be separated during the streamline simulations and to prevent any possible interference, only the paired-well data (1 km distance) have been included within the results. Flow rates and well pressures from both producers and injectors were based on well data from the Glitne Field and kept the same between different realisations, in order to allow constant pressure and reservoir conditions for the performance of streamline simulations.

STREAMLINE SIMULATION RESULTS

Basin floor lobe complex (BFL)

Simulation results of Model A (coarsening- and thickening-upwards) and Model B (facies transitions) (Fig. 11) are compared using TBT histograms (Fig. 13) that show the spread in breakthrough times between injector-producer pairs in different realisations. These different realisations are the result of the stochastic approach on the petrophysical modelling (Fig. 2). Within Model A, the timing of breakthrough is similar for both locations, but with a slightly larger spread at the ‘Fringe’ location. In Model B, however, the breakthrough at the ‘Axis’ is on average more than a year (1.3) later than at the ‘Fringe’. Two-tail t-tests (0.05 significance level), assuming unequal variances, confirms that the results from both locations are distinctive populations (Fig. 13). Drainage functions performed for Model A & B at the ‘Axis’ (five per model) indicates that within Model B production rates are significantly higher directly from the start of production and that cumulative production is on average over 40% higher (Fig. 14) after the first 40 years. Timing of breakthrough between Model B1 and B2 is similar at both well locations, which is confirmed by two-tailed t-tests (Fig. 13). However, the TBT results of Model B3 (Fig. 13), show a significantly reduced average breakthrough time at the ‘Axis’ (confirmed by t-test – Fig. 13) of 2 years compared to Model B2. The wells at the ‘Fringe’ within Model B3 on the other hand show very similar results to Model B2. Furthermore, a substantial difference (~60% in 40 years) in cumulative production can be observed between the ‘Axis’ and the ‘Fringe’ in Model B (B2) within a lobe complex (Fig. 14).

CLTZ Models

The TBT results of the OR and BLK models have been summarised in Figure 15. Within the upscaled version of the OR-model (OR-A), breakthrough takes longer (2-3 years) for all well locations compared to the more realistic sub-model (OR-B). Within OR-B, the timing of breakthrough is not only shorter but also more uniform at the different well pairs. Within both the OR-A and OR-B simulations, streamlines from all wells are observed to focus along the main channel-fill sandstones (Fa1A) (Fig. 15).

Similar effects on TBT can be observed between BK Ch1 and BK Ch2 with an average decrease of breakthrough time of 4 years. The non-channelised model (BK no-Ch) shows minimal differences with slightly shorter breakthrough timing compared to BK Ch1 confirmed by a t-test (Fig. 15). Drainage functions have also been performed and show distinct variation between the submodels after the first 10 years (Fig. 15). The lowest production rates are reached within (BK Ch2), while the highest production rates are seen within the non-channelised model (BK no-Ch). However, differences within cumulative production between the submodels are limited (3-8% in 40 years) and only become significant after the first 20 years. Active pore volume has also been calculated for the BK-models, to see if part of the observed production differences could be related to differences in reservoir volume. Active pore volume is the segment of the total pore volume that can be produced from, before breakthrough occurs. Differences between BK Ch1 ($3.34\text{x}10^6\ m^3$) and BK Ch2 ($3.30\text{x}10^6\ m^3$) are minimal. However, by removing the channels completely (BK no-Ch – $3.05\text{x}10^6\ m^3$), active pore volume was reduced by more than 8%. This indicates that total reservoir volume is not the controlling factor as the models with the largest active pore volume (BK Ch1 & BK Ch2) show lower production rates.

DISCUSSION

Interpreting streamline simulation results

The single phase-flow experiments were designed to study the relative differences in connectivity within reservoirs. A slow breakthrough time of the injected fluid within the producer well indicates that the injector and producer are poorly connected within the reservoir, which can have negative consequences for production rates. On the other hand, early breakthrough often has negative implications for recovery factors due to expensive water cycling and low vertical sweep efficiency within the reservoir (e.g. Brouwer *et al.* 2001; Brouwer & Jansen 2002; Alhuthali *et al.* 2006). Therefore, the sensitivity studies and their implications on the timing of breakthrough can help to rank different probable scenarios of reservoir performance. When breakthrough times have proven to be distinct (t-test) between sub-model results, it shows that the effect of the change applied in the facies model is significant enough to be discriminated from the uncertainty associated with petrophysical properties. A higher uncertainty (high standard deviation) within the results is mostly related to the greater impact and uncertainty within the low-permeable deposits on the connectivity of the system, compared to the high-permeable deposits. The use of simplistic reservoir models, before adding more complicated variables is widely referred to as 'top-down modelling' (e.g. Williams et al., 2004). By adding more variables to simplistic models, a large variety of different scenarios can be created which can highlight the most significant uncertainties, called 'procycling' (Larue & Hovadik, 2012). Procycling is considered a useful process for uncertainty analysis, especially for deep-water reservoirs (Larue & Hovadik, 2012; Saikia *et al*., 2015).

Basin floor lobe complex (BFL)

The modelling results of the medial to distal basin floor lobe complex (BFL) show that the choice of conceptual geological model (Model A or B) has a major influence on the best well placement strategy. Within Model B, there is a clear difference observed in both breakthrough time and production from the axial lobe complex areas (Axis) compared to more fringe positions (Fringe). This is related to the lateral facies changes that have been implemented within Model B and are not present within Model A. Furthermore, Model B has a significantly better production rate (Fig. 14). This is largely related to the petrophysical property differences between the two models as the nature of Model A with all lobe zones stacked in combination with the facies maps will result in different facies proportions. The average permeability of Model B (156 mD) is therefore over 50% higher than within Model A (92 mD), which will impact production results. Reservoir performance differences are therefore related to both the facies structure as well as facies proportions differences related to the conceptual models applied within Model A and B. The B-submodels indicate that facies changes applied within the off-axis/fringe environments do not significantly influence the connectivity of the system (B1 & B2). Changes applied in the axis of the lobes (B3), where lobe amalgamation occurs, have a much more significant impact. In this case, the addition of Fa2 within the axial lobe areas improved the vertical connectivity, even though its volume was limited (14.3% of axis – Fig. 7). Also, the results demonstrate that when heterogeneity is increased within the axial areas, performance differences between well locations are less apparent. The adjustments within lobe style modelling of the BFL models prove to have significant impact on predicted reservoir performance. In many cases, this uncertainty in modelling of sedimentary architecture is more significant than the large uncertainties associated with the petrophysical modelling (spread in TBT results).

CLTZ Models

The results from the CLTZ-block model indicate that channel-fills within channelised lobe areas can have a variable effect on reservoir performance. Wells within the coarse, upscaled version of the OR-model (OR-A) take more than 3 times longer to reach breakthrough compared to the downscaled version (OR-B). In both the detailed model (OR-B) and the upscaled version (OR-A), fluid flow streamlines concentrate within the channel-fills (Fig. 15A). However, the heterogeneities of the minor facies associations within OR-B have a major effect on pressure concentration, which results in the compartmentalisation of the reservoir, indicated by the early breakthrough.

The BK-model confirms that heterogeneities within minor facies groups of channel-fills have substantial impact on reservoir connectivity. Differences in performance between BK Ch1 and BK Ch2 are also related to vertical compartmentalisation of the reservoir, resulting in early breakthrough. The similarity in results of BKCh1 and BK No-Ch also indicates that the channel-fills only have a limited influence on the performance of the reservoir. In addition, according to the drainage functions (Fig. 15A), the channel fills still have a slightly negative effect on production when they are well-connected (BK Ch1) with the background deposits (lobes and overbank), compared to when no channel fills are present (BK No-Ch). The more favourable petrophysical properties of the channel-fill facies (Fa1A) (Fig. 10) compared to the sand-prone and volumetrically larger background deposits will in both the BK Ch1 and the BK Ch2 (Fig. 8) cases act as a pressure leak, which reduces the drainage area of the reservoir. Production differences between the three cases are mostly due to the full vertical injection and production, which ensures injection and production over the whole vertical interval. Production differences could well become more significant if injection or production would not occur over the complete reservoir interval, as vertical permeability boundaries will become much more important.

Implications on reservoir performances within CLTZ environments

Stratigraphic juxtaposition of basin-floor channels and lobes, such as observed in the Tanqua depocentre outcrops (e.g. Luthi *et al.* 2006; Fig. 5A), has a variable effect on reservoir performance (Fig.15B), and depends on the nature of the lobe deposits and the presence of flow barriers or baffles at the base of and within the channel-fills. With injection over the full vertical thickness of the fan, interlobe (distal fringe) heterogeneities do not have much effect when the deposits are sufficiently sand-prone. Other factors such as inter-channel barriers have proven to substantially change reservoir predictions (Fig. 15). These barriers include channel bases that are at least partly overlain by mudstone clast conglomerates. As these mudstone clast conglomerates could provide high permeability in the case of matrix-supported types but very low permeability in the case of clast-supported types, a wide range in permeability (10-5000 mD) has to be accounted for. Furthermore, the impact of heterogeneities caused by (partly) argillaceous sandstones have been considered. OR-B and BK-B both show a clear overall switch to early breakthrough with the addition of these vertical heterogeneities (Fig. 15B). This shows that the combination of multiple heterogeneous facies groups can influence flow pathways within the reservoir.

However, these intra-channel barriers (consistent basal mudstone clast conglomerate layer and argillaceous sandstones in the top of the fill) that have been added in the CLTZ submodels (OR-B and BK Ch2) may represent an end member scenario as basin-floor channel-fills show limited spatial variety and variability between channel-fills (e.g. Brunt *et al.* 2013). According to Alpak *et al.* (2013), the presence of mud drapes, including mudstone clast-conglomerates, at the channel-base is most important when assessing recovery factors. However, the probability of channel bases overlain by mudstones in base-of-slope and basin-floor settings according to Alpak *et al.* (2013) is significantly less (<10%) than compared to slope channel-fills where mudstone drapes across the base of channels are more common and interpreted to indicate sediment bypass (e.g. Barton *et al.* 2010; Hubbard *et al.* 2014; Stevenson *et al.* 2015). Eschard *et al.* (2014) observed lenses of matrix-supported (claystone) materials in their study of the basin floor system of the Pab Formation and noted that the lateral extension of these units is commonly limited. In the case of Eschard *et al.* (2014), the flow streamlines were able to bypass the heterogeneities due to local erosion and therefore only had limited impact. This implies that even though the channels within a channelised lobe area (CLTZ) are considered to have better connected margins compared to upslope channel-levee systems (Funk *et al.* 2012; Alpak *et al.* 2013), there is a great level of uncertainty accompanying the behaviour of these boundaries and associated performance of CLTZ-reservoirs. Due to the combination of relatively low total volumes of channel-fills compared to surrounding deposits including lobes, the distributive character and the uncertainty within channel-fill behaviour, channelised-lobe environments may be considered as a higher risk as an exploration target than conventional ideas might suggest.

Alternative areas of better vertical connectivity are high amalgamation zones (Stephens *et al.* 2001; Hodgetts *et al.* 2004; Hodgson *et al.* 2006) at lobe apexes. Within these areas there is an overall lower chance of reservoir compartmentalisation compared to channelised lobe areas, due to the lack of horizontal flow barriers. Also the impact of abrupt facies changes (in the case of an erosive barrier) compared to gradual facies changes (in the case of facies transitions), may have important consequences for the pressure distribution and fluid migration rates. The BFL model results show that amalgamation of lobe axes has a significant impact on reservoir performance.

Ranking reservoir performance

Streamline simulations are commonly used for ranking reservoir performance before more comprehensive flow simulations are initiated (e.g. Idrobo *et al.* 2000) and can also be used when complicated grids or high number of grid cells make flow simulation challenging. Comparing the macroscopic sweep efficiency between the different scenarios gives a good indication of problem areas as well as identifying the areas of interest for exploration within deep-marine fan systems. The well-constrained depositional architecture of the Karoo Basin lobe complexes (Hodgson *et al.* 2006; Prélat *et al.* 2009), further understanding from the modelling results of this study, and previous stochastic modelling results (e.g. Stephens *et al.* 2001; Funk *et al.* 2012; Alpek *et al.* 2013), have been integrated to develop a model on recovery (macroscopic sweep) efficiency within basin-floor fan systems. A division has been implemented based on sub-environments (Fig. 16): channelised lobe, amalgamated lobe and non-amalgamated lobe areas. Different scenarios have been attributed to each sub-environment linked to heterogeneity differences. Macroscopic sweep efficiency has been linked to the timing of breakthrough. As only for a limited number of models drainage functions (Fig. 14; 15) were run, the general assumption was made that both slow and rapid breakthrough will result in relatively low recovery with limited drainage areas. A good non-compartmentalised and connected reservoir with good-to-intermediate porosity will result in the best total recovery. The most variability in performance can be seen among the channelised lobe areas (CLTZ) (Fig. 16, circles). The possibility of both compartmentalised and non-compartmentalised channelised lobes, makes the prediction of macroscopic sweep efficiency within these environments more challenging. Less uncertainty is associated with amalgamated lobe areas (Fig. 16, pentagons) where good vertical and horizontal connectivity are predicted. Amalgamated lobe areas as a reservoir will therefore have higher chances of good recovery rates and will be less of an exploration risk compared to channelised lobe areas.

CONCLUSIONS

A 3-D geological modelling workflow is presented from outcrop data collection, through constructing reservoir models to performing single-phase flow simulations. The workflow highlights the importance of understanding fine-scale sub-seismic sedimentary architecture. Various sensitivity tests were performed by applying geologically realistic scenarios for sedimentary architecture and facies distributions of submarine lobe deposits and channel-fills. Results show that the conceptual model applied for a specific case study can have significant influence on the reservoir connectivity and macroscopic sweep efficiency, especially when lobe amalgamation is considered. The implications on connectivity by alternations in facies within the high net lobe axis areas are much more significant compared to similar changes within lobe off-axis to fringe areas. Juxtaposition of channel-fills and lobe deposits, which is common in CLTZs, has diverse effects on reservoir performance depending on the presence of inter-channel barriers and the sand-prone nature of the lobes. In CLTZs, due to the high degree of uncertainty of heterogeneities associated with channelised lobe areas, they can be considered a more challenging production target compared to areas of lobe amalgamation where good horizontal and vertical connectivity are more certain. For the construction of geologically realistic reservoir models, it remains vital to collect quantitative data from fine-scale architectures within outcrop analogues, which may form significant reservoir heterogeneities, and to develop and test conceptual models, such as can be done with the well-constrained basin-floor fan systems of the Karoo Basin.

ACKNOWLEDGEMENTS

We are especially grateful to the support of Statoil for providing the opportunity to use their facilities at the Rotvoll office at Trondheim. Outcrop studies were carried out as part of the LOBE 2 consortium research project. We are grateful for the financial support from: Anadarko, Bayerngas Norge, BG Group, BHP Billiton, BP, Chevron, Dong Energy, engie, E.ON, Maersk Oil, Marathon Oil, Shell, Statoil, Total, VNG Norge and Woodside. We are grateful to Michael Pyrcz and Mark Bentley for their constructive reviews, which greatly improved this manuscript. We also acknowledge the landowners in the Tanqua area for permission to access their land. Finally, Renée de Bruijn and Nienke Lips are thanked for their assistance in the field and Yvonne Spychala for her contributions to Figure 7.

REFERENCES

Aarnes, J.E., Krogstad, S. & Lie, K-A., 2008. Multiscale mixed/mimetic methods on corner-point grids. *Computational Geosciences*, **12**, 297-315.

Alabert, F.G. & Massonnat, G.J., 1990. Heterogeneity in a complex turbiditic reservoir: stochastic modelling of facies and petrophysical variability. *SPE Annual Technical Conference and Exhibition*. Society of Petroleum Engineers, SPE 20604.

Alpak, F.O., Barton, M.D. & Naruk, S.J., 2013. The impact of fine-scale turbidite channel architecture on deep-water reservoir performance. *AAPG Bulletin*, **97**, 251-284.

Alhuthali, A., Oyerinde, A. & Datta-Gupta, A., 2006. Optimal waterflood management using rate controls. *SPE Annual Technical Conference and Exhibition*. SPE 102478-MS.

Amy, L.A., Peachey, S.A., Gardiner, A.R., Pickup, G.E., Mackay, E. & Stephen, K.D., 2013. Recovery efficiency from a turbidite sheet system: numerical simulation of waterflooding using outcrop-based geological models. *Petroleum Geoscience*, **19**, 123-138.

Avseth, P., Mukerji, T., Jørstad, T., Mavko, A. & Veggeland, T., 2001. Seismic reservoir mapping from 3-D AVO in a North Sea turbidite system. *Geophysics*, **66**, 1157-1176.

Barton, M., O’Byrne, C., Pirmez, C., Prather, B., Van der Vlugt, F., Alpak, F.O. & Sylvester, Z., 2010. Turbidite channel architecture: Recognizing and quantifying the distribution of channel-base drapes using core and dipmeter data. *In:* Pöppelreiter, M., García-Carballido, C., Kraaijveld, M. (eds) *Dipmeter and bore-hole image log technology: AAPG Memoir*, **92**, 195-210.

Beaubouef, R.T, Van Wagoner, J.C. & Adair, N.L., 2003. Ultra-high resolution 3-D characterization of deep-water deposits-II: Insights into the evolution of a submarine fan and comparisons with river deltas, *AAPG Annual Meeting*, *Extended Abstracts*, May 11-14.

Bennes, M. & Hamon, G., 2007. Core petrophysical synthesis carried out at a scale of a basin, some examples from Tertiary offshore reservoirs. *Society of Core Analysts, SCA*, **27**, 1-12.

Bouma, A. & Wickens, H.d.V., 1991. Permian passive margin submarine fan complex, Karoo Basin, South Africa: Possible model to Gulf of Mexico, *Gulf Coast Association of Geological Societies Transactions*, **41**, 30-42.

Bouma, A. & Wickens, H.d.V., 1994. Tanqua Karoo, ancient analog for fine-grained submarine fans. *In:* P. Weimer, A.H. Bouma & B.F. Perkins (eds) *Submarine Fans and Turbidite Systems: Sequence Stratigraphy, Reservoir Architecture, and Production Characteristics: Gulf Coast Section SEPM Foundation 15th Research Conference Proceedings*, pp. 23-34.

Brandsæter, I., Wist, H.T., Næss, A., Lia, O.A., Ole, J., Ringrose, P.S., Martinius, A.W., Lerdahl & T.R., 2001. Ranking of stochastic realizations of complex tidal reservoirs using streamline simulation criteria. *Petroleum Geoscience*, **7**, S53-S63.

Brouwer, D.R. & Jansen, J.D., 2002. Dynamic optimization of water flooding with smart wells using optimal control theory. *SPE European Petroleum Conference,* SPE 78278.

Brouwer, D.R., Jansen J.D., Van der Starre, S., Van Kruijsdijk, C.P.J.W. & Berentsen, C.W.J., 2001. Recovery increase through water flooding with smart well technology. *SPE European Formation Damage Conference,* SPE 68979.

Brunt, R.L., Hodgson, D.M., Flint, S.S., Pringle, J.K., Di Celma, C., Prélat, A. & Grecula, M., 2013. Confined to unconfined: anatomy of a base of slope succession, Karoo Basin, South Africa. *Marine and Petroleum Geology*, **41**, 206-221.

Bryant, I.D. & Flint, S.S., 1993. Quantitative clastic reservoir geological modelling: problems and perspectives. *In:* Flint, S.S. & Bryant, I.I., (eds). The geological modelling of hydrocarbon reservoirs and outcrop analogues. *Int. Assoc. Sedimentol. Spec. Publ.*, **15**, 3-20.

Clark, J.D. & Pickering, K. T., 1996. Architectural elements and growth patterns of submarine channels: application to hydrocarbon exploration. *AAPG Bulletin*, **80**, 194-220.

De Wit, M.J. & Ransome, I.G., 1992. Regional inversion tectonics along the southern margin of Gondwana. *In:* De Wit, M.J., Ransome, I.G.D. (eds) *Inversion Tectonics of the Cape Fold Belt, Karoo and Cretaceous Basins of Southern Africa*. Amsterdam, Balkema, 15-22.

Deptuck, M.E., Piper, M.E., David, J.W., Savoye, B. & Gervais, A., 2008. Dimensions and architecture of late Pleistocene submarine lobes off the northern margin of East Corsica. *Sedimentology*, **55**, 869-898.

Drinkwater, N.J. & Pickering, K.T., 2001. Architectural elements in a high-continuity sand-prone turbidite system, late Precambrian Kongsfjord Formation, northern Norway: Application to hydrocarbon reservoir characterization. *AAPG Bulletin*, **85**, 1731-1757.

Eschard, R., Deschamps, R., Dobligez, B., Lerat, O., Langlais, V. & Euzen, T., 2014. Connectivity estimation between turbiditic channels and overbank deposits from the modelling of an outcrop analogue (Pab Formation, Maastrichtian, Pakistan). *In:* Martinius, A.W., Howell, J.A. & Good, T.R. (eds) *Sediment-Body Geometry and Heterogeneity: Analogue Studies for Modelling the Subsurface.* Geological Society, London, Special Publications, **387**, 203-231.

Falivene, O., Arbués, P., Howell, J., Muñoz, J.A., Fernández, O. & Marzo, M., 2006. Hierarchical geocellular facies modelling of a turbidite reservoir analogue from the Eocene of the Ainsa Basin, NE Spain. *Marine and Petroleum Geology*, **23**, 679-701.

Fildani, A., Weislogel, A., Drinkwater, N.J., McHargue, T., Tankard, A., Wooden, J., Hodgson, D.M. & Flint, S.S., 2009. U-Pb zircon ages from the southwestern Karoo Basin, South Africa – Implications for the Permian-Triassic boundary. *Geology*, **37**, 719-222.

Flint, S.S., Hodgson, D.M., Sprague, A., Brunt, R.L., Van Der Merwe, W.C., Figueiredo, J., Prélat, A., Box, D., Di Celma, C. & Kavanagh, J.P., 2011. Depositional architecture and sequence stratigraphy of the Karoo basin floor to shelf edge succession, Laingsburg depocentre, South Africa. *Marine and Petroleum Geology*, **28**, 658-674.

Funk, J.E., Slatt, R.M. & Pyles, D.R., 2012. Quantification of static connectivity between deep-water channels and stratigraphically adjacent architectural elements using outcrop analogs. *AAPG Bulletin*, **96**, 277-300.

Groenenberg, R.M., Hodgson, D.M., Prélat, A., Luthi, S.M. & Flint, S.S., 2010. Flow-deposit interaction in submarine lobes: Insights from outcrop observations and realizations of a process-based numerical model. *Journal of Sedimentary Research*, **80**, 252-267.

Hewett, T.A., 1986. Fractal distributions of reservoir heterogeneity and their influence on fluid transport. *SPE Annual Technical Conference and Exhibition*, Society of Petroleum Engineers, SPE 15386.

Hodgetts, D., Drinkwater, N.J., Hodgson, D.M., Kavanagh, J., Flint, S.S., Keogh, K.J. & Howell J.A., 2004. Three-dimensional geological models from outcrop data using digital data collection techniques: an example from the Tanqua Karoo depocentre, South Africa. *In:* Curtis, A.C. & Wood, R. (eds) *Geological Prior Information: Informing Science and Engineering.* Geological Society, London, Special Publications, **239**, 57-75.

Hodgson, D.M., 2009. Distribution and origin of hybrid beds in sand-rich submarine fans of the Tanqua depocentre, Karoo Basin, South Africa. *Marine and Petroleum Geology*, **26**, 1940-1956.

Hodgson, D.M., Flint, S.S., Hodgetts, D., Drinkwater, N.J., Johannessen, E.P. & Luthi, S.M., 2006. Stratigraphic evolution of fine-grained submarine fan systems, Tanqua depocenter, Karoo Basin, South Africa. *Journal of Sedimentary Research*, **76**, 20-40.

Hofstra, M., Hodgson, D.M., Peakall, J. & Flint, S.S., 2015. Giant scour-fills in ancient channel-lobe transition zones: Formative processes and depositional architecture. *Sedimentary Geology*, **329**, 98-114.

Hovadik, J.M. & Larue, D.K., 2007. Static characterizations of reservoirs: refining the concepts of connectivity and continuity. *Petroleum Geoscience*, **13**, 195-211.

Howell, J.A., Martinius, A.W. & Good, T.R., 2014. The application of outcrop analogues in geological modelling: a review, present status and future outlook*. In:* Martinius, A.W., Howell, J.A., Good, T.R. (eds) *Sediment-Body Geometry and Heterogeneity: Analogue Studies for Modelling the Subsurface.* Geological Society, London, Special Publications, **387**, 135-151.

Hubbard, S.M., Covault, J.A., Fildani, A. & Romans, B.W., 2014. Sediment transfer and deposition in slope channels: Deciphering the record of enigmatic deep-sea processes from outcrop. *Geological Society of America Bulletin*, **126**, 857-871.

Idrobo, E.A., Choudhary, M.K. & Datta-Gupta, A., 2000. Swept volume calculations and ranking geostatistical reservoir models using streamline simulation. *SPE/AAPG Western Regional Meeting.* Society of Petroleum Engineers. SPE 62557.

Jackson, M., Percival, J., Mostaghimi, P., Tollit, B., Pavlidis, D., Pain, C. & Blunt, M., 2015. Reservoir modelling of flow simulation by use of surfaces, adaptive unstructured meshes, and an overlapping-control-volume finite-element method. *SPE Reservoir Evaluation & Engineering*. Doi: 10.2118/163633-PA

Johnson, S.D., Flint, S.S., Hinds, D. & Wickens, H.d.V., 2001. Anatomy, geometry and sequence stratigraphy of basin floor to slope turbidite systems, Tanqua Karoo, South Africa. *Sedimentology*, **48**, 987-1023.

Joseph, P., Babonneau, N., Bourgeois, A., Cotteret, G., Eschard, R., Garin, B., Granjeon, D., Lerat, O., Ravenne, C., Gomes de Souza, O., Guillocheau, F. & Quemener, J., 2000. The Annot Sandstone outcrops (French Alps): Architecture description as input for quantification and 3-D reservoir modelling. *In:* Weimer, P., Slatt, R.M., Coleman, J., Rosen, N.C., Nelson, H., Bouma, A.H., Styzen, M.J., Lawrence, D.T. (eds) *Deep-Water Reservoirs of the World: Gulf Coast Section SEPM Foundation 20th Annual Research Conference*, **28**, 422-449.

Kane, I.A. & Pontén, A.S.M., 2012. Submarine transitional flow deposits in the Palaeogene Gulf of Mexico. *Geology*, **40**, 1119-1122.

Keogh, K.J., Berg, F.K. & Glitne Petek, 2008. A method for quantifying geological uncertainties in assessing remaining oil targets: a case study from the Glitne Field, North Sea. *In:* Robinson, A., Griffiths, P., Price, S., Hegre, J., Muggeridge, A. (eds) *The Future of Geological Modelling in Hydrocarbon Development,* Geological Society, London, Special Publications, **309**, 193-203.

Kirschner, R.H. & Bouma, A.H., 2000. Characteristics of a distributary channel-levee-overbank system, Tanqua Karoo. *In*: Bouma, A.H. & Stone, J. (eds) *Fine-Grained Turbidite Systems*, *AAPG Memoir,* **80**, 337-364.

Kleverlaan, K. & Cossey, S.P.J., 1993. Permeability barriers within sand-rich submarine fans: outcrop studies of the Tabernas Basin, SE Spain. *In:* Eschard, R. & Doligez, B. (eds) *Subsurface Reservoir Characterisation from Outcrop Observations*: Editions Technip, Paris, 161-164.

Labourdette, R., Devilliers, M.C. & Bui, T., 2013. History match of a DST using a turbidite elementary channels modelling technique, deep offshore Congo. SPE Reservoir Characterization and Simulation Conference and Exhibition. Society of Petroleum Engineers.

Larue, D.K., 2004. Outcrop and waterflood simulation modeling of the 100-foot channel complex, Texas, and the Ainsa II channel complex, Spain: Analogs to multistory and multilateral channelized slope reservoirs. *In:* Grammer, M., Harris, P.M. & Eberli, G.P. (eds) *Integration of outcrop and modern analogs in reservoir modelling*, AAPG Memoir, **80**, 337-364.

Larue, D. K. & Friedmann, F., 2005. The controversy concerning stratigraphic architecture of channelized reservoirs and recovery by waterflooding. *Petroleum Geoscience*, **11**, 131-146.

Larue, D.K. & Hovadik, J., 2012. Rapid earth modelling for appraisal and development studies of deep-water clastic reservoirs and the concept of 'procycling'. *Petroleum Geoscience*, **18**, 201-218.López-Gamundí, O.R. & Rossello, E.A., 1998. Basin fill evolution and paleotectonic patterns along the Samfrau geosyncline: the Sauce Grande basin–Ventana foldbelt (Argentina) and Karoo basin–Cape foldbelt (South Africa) revisited. *Geologische Rundschau*, **86**, 819-834.

Luthi, S.M., Hodgson, D.M., Geel, C.R., Flint, S.S., Goedbloed, J.W., Drinkwater, N.J. & Johannessen, E.P., 2006. Contribution of research borehole data to modelling fine-grained turbidite reservoir analogues, Permian Tanqua-Karoo basin-floor fans (South Africa). *Petroleum Geoscience*, **12**, 175-190.

Macdonald, H.A., Peakall, J., Wignall, P.B. & Best, J., 2011. Sedimentation in deep-sea lobe-elements: Implications for the origin of thickening-upward sequences. *Journal of the Geological Society of London*, **168**, 319-331.

Mayall, M., Jones, E. & Casey, M., 2006. Turbidite channel reservoirs – key elements in facies prediction and effective development. *Marine and Petroleum Geology*, **23**, 821-841.

McKay, M.P., Weislogel, A.L., Fildani, A., Brunt, R.L., Hodgson, D.M. & Flint, S.S., 2015. U-PB zircon tuff geochronology from the Karoo Basin, South Africa: implications of zircon recycling on stratigraphic age controls. *International Geology Review*, **57**, 393-410.

Mutti, E., 1977. Distinctive thin-bedded turbidite facies and related depositional environments in the Eocene Hecho Group (South-central Pyrenees, Spain). *Sedimentology*, **24**, 107-131.

Mutti, E. & Sonnino, M., 1981. Compensation cycles: a diagnostic feature of sandstone lobes. Int. Assoc. Sediment., 2nd Europ. Meeting, Bologna, Abstr., 120-123.

Piper, D.J.W. & Normark, W.R., 1983. Turbidite depositional patterns and flow characteristics, Navy Submarine Fan, California Borderland. *Sedimentology,* **30**, 681-694.

Pirmez, C., Beaubouef, R.T., Friedmann, S.J. & Mohrig, D.C., 2000. Equilibrium profile and baselevel in submarine channels: examples from Late Pleistocene systems and implications for the architecture of deepwater reservoirs. *In:* Weimer, P., Slatt, R.M., Coleman, J., Rosen, N.C., Nelson, H., Bouma, A.H., Styzen, M.J. & Lawrence, D.T. (eds) *Deep water reservoirs of the world*, GCSSEPM Foundation, Houston, 782-805.

Prélat, A., 2010. Evolution, architecture and hierarchy of distributary deepwater deposits: a high resolution outcrop investigation of submarine lobe deposits from the Permian Karoo Basin, South Africa. *Unpublished PhD Thesis,* University of Liverpool, pp. 317.

Prélat, A. & Hodgson, D.M., 2013. The full range of turbidite bed thickness patterns in submarine lobes: controls and implications. *Journal of the Geological Society*, **170**, 209-214.

Prélat, A., Hodgson, D.M. & Flint, S.S., 2009. Evolution, architecture and hierarchy of distributary deep-water deposits: a high-resolution outcrop investigation from the Permian Karoo Basin, South Africa. *Sedimentology*, **56**, 2132-2154.

Prélat, A., Covault, J.A., Hodgson, D.M., Fildani, A. & Flint, S.S., 2010. Intrinsic controls on the range of volumes, morphologies, and dimensions of submarine lobes. *Sedimentary Geology*, **232**, 66-76.

Pringle, J.K., Brunt, R.L., Hodgson, D.M. & Flint, S.S., 2010. Capturing stratigraphic and sedimentological complexity from submarine channel complex outcrops to digital 3D models, Karoo Basin, South Africa. *Petroleum Geoscience*, **16**, 307-330.

Pringle, J.K., Howell, J.A., Hodgetts, D., Westerman, A.R. & Hodgson, D.M., 2006. Virtual outcrop models of petroleum reservoir analogues: a review of the current state-of-the-art. *First Break*, **24**, 33-42.

Pyrcz, M.J. & Deutsch, C.V., 2014. Geostatistical reservoir modelling, Oxford University Press, 448 pp.

Pyrcz, M.J., Catuneanu O. & Deutsch, C.V. 2005. Stochastic surface-based modeling of turbidite lobes. *AAPG Bulletin*, **89**, 177-191.

Ricci-Lucchi, F., 1975. Depositional cycles in two turbidite formations of Northern Apennines (Italy). *Journal of Sedimentary Petrology*, **45**, 3-43.

Richards, M. & Bowman, M., 1998. Submarine fans and related depositional systems II: variability in reservoir architecture and wireline log character. *Marine and Petroleum Geology*, **15**, 821-839.

Ringrose, P. & Bentley, M., 2015. Reservoir Model Design. Springer, 249 pp.

Saikia, K., Khan, W. & Ramakrishnan, S., 2015. Challenges in deepwater reservoir characterization: From well log interpretation and well testing to 3D geocellular modelling. *SPE Annual Technical Conference and Exhibition*, Society of Petroleum Engineers, SPE 175071.Saller, A., Werner, K., Sugiaman, F., Fransiskus, C.A., May, R., Glenn, D. & Craig, B., 2008. Characteristics of Pleistocene deep-water fan lobes and their application to an upper Miocene reservoir model, offshore East Kalimantan, Indonesia. *AAPG Bulletin*, **92**, 919-949.

Scaglioni, P., Ruvo, L. & Cozzi, M., 2006. Implicit net-to-gross in the petrophysical characterization of thin-layered reservoirs. *Petroleum Geoscience*, **12**, 325-333.

Schwarz, E. & Arnott, R.W.C., 2007. Anatomy and evolution of a slope channel-complex set (Neoproterozoic Isaac Formation, Windermere Supergroup, southern Canadian Cordillera): implications for reservoir characterizations. *Journal of Sedimentary Research*, **77**, 89-109.

Shanmugam, G. & Moiola, R.J., 1991. Types of Submarine Fan Lobes: Models and Implications (1). *AAPG Bulletin*, **75**, 156-179.

Sprague, A.R.G., Garfield, T.R., Goulding, F.J., Beaubouef, R.T., Sullivan, M.D., Rossen, C., Campion, K.M., Sickafoose, D.K., Abreu, V., Schellpeper, M.E., Jensen, G.N., Jennette, D.C., Pirmez, C., Dixon, B.T., Ying, D., Ardill, J., Mohrig, D.C., Porter, M.L., Farrell, M.E. & Mellere, D., 2005. Integrated slope channel depositional models: the key to successful prediction of reservoir presence and quality in offshore west Africa. *CIPM, cuarto E-Exitep*. pp. 1—13.

Stephen, K.D., Clark, J.D. & Gardiner, A.R., 2001. Outcrop-based stochastic modelling of turbidite amalgamation and its effects on hydrocarbon recovery. *Petroleum Geology*, **7**, 163-172.

Stevenson, C.J., Jackson, C.A.L., Hodgson, D.M., Hubbard, S.M. & Eggenhuisen, J.T., 2015. Deep-water sediment bypass. *Journal of Sedimentary Research*, **85**, 1058-1081.

Stow, D.A. & Johansson, M., 2000. Deep-water massive sands: nature, origin and hydrocarbon implications. *Marine and Petroleum Geology*, **17**, 145-174.

Straub, K.M. & Pyles, D.R., 2012. Quantifying the hierarchical organization of compensation in submarine fans using surface statistics. *Journal of Sedimentary Research*, **82**, 889-898.

Strebelle, S., Payrazyan, K. & Caers, J., 2003. Modeling of a deepwater turbidite reservoir conditional to seismic data using principal component analysis and multiple-point geostatistics. *SPE Journal*, **8**, 227-235.

Sullivan, M., Jensen, G., Goulding, F., Jennette, D., Foreman, L. & Stern, D., 2000. Architectural analysis of deep-water outcrops: Implications for exploration and development of the Diana sub-basin, western Gulf of Mexico. *In:* Weimer, P., Slatt, R.M., Coleman, J., Rosen, N.C., Nelson, H., Bouma, A.H., Styzen, M.J. & Lawrence, D.T. (eds) *Deep Water Reservoirs of the World*, GCSSEPM Foundation, Houston, 1010-1032.

Sullivan, M.D., Foreman, J.L., Jennette, D.C., Stern, D., Jensen, G.N. & Goulding, F.J., 2004. An integrated approach to characterization and modelling of deep-water reservoirs, Diana field, western Gulf of Mexico. *AAPG Memoir*, **80**, 215-234.

Van der Werff, W. & Johnson, S., 2003. High resolution stratigraphic analysis of a turbidite system, Tanqua Karoo Basin, South Africa. *Marine and Petroleum Geology*, **20**, 45-69.

Veevers, J.J., Cole, D. I. & Cowan, E.J., 1994. Southern Africa: Karoo basin and Cape fold belt. *In:* Veevers, J.J. & Powell, C.Mc.A. (eds) *Permian-Triassic Pangean basins along the Panthalassan margin of Gondwanaland: Geological Society of America Memoir*, **184**, 223-279.

Wild, R., Flint, S.S., & Hodgson, D.M., 2005. Architecture and stratigraphic evolution of multiple, vertically-stacked slope channel compexes, Tanqua depocentre, Karoo Basin, South Africa. *In:* Hodgson, D.M. & Flint, S.S. (eds). Submarine Slope Systems: Processes and Products, *Geological Society, London, Special Publication*, **244**, 89-111.

Williams, G.J.J., Mansfield, M., McDonald, D.G. & Bush, M.D., 2004. Top-down reservoir modelling. *SPE Annual Technical Conference and Exhibition*, Society of Petroleum Engineers, SPE 89974.

Zhang, X.,Pyrcz, M.J. & Deutsch, C.V., 2009. Stochastic surface modeling of deepwater depositional systems for improved reservoir models. *Journal of Petroleum Science and Engineering*, **68**, 118-134.

Zou, F., Slatt, R., Bastidas, R. & Ramirez, B., 2012. Integrated outcrop reservoir characterization, modelling, and simulation of the Jackfork Group at the Baumgartner Quarry area. *AAPG Bulletin*, **96**, 1429-1448.

Figure captions

Fig 1. Simplified cartoon of a basin-floor submarine lobe complex showing distinct subenvironments with A – confined channel systems, B – distributive channel network, C – high amalgamation zone (HAZ), D – distal lobe environment. Based on Kane & Pontén 2012.

Fig. 2. Illustration of the complete workflow that has been followed, including geological modelling, reservoir modelling and flow simulation. All data input is indicated by arrows. The table shows the main uncertainties within each modelling step, the number of submodels produced, how the uncertainties were covered, and why multiple models were required. **'**CLTZ' refers to channel lobe transition zone, 'BFL' to basin floor lobe complex model, 'OR' and 'BK' to the 'Ongeluks River' and 'Blaukop' datasets respectively, and 'Ch' and 'no-Ch' to channels and no-channels respectively – see text for further details.

Fig.3. Location map of the Tanqua depocentre showing the outcrop analogues that have been used for facies modelling and the stratigraphic column of the Tanqua deep-water deposits (based on Hofstra *et al.* 2015). The basin floor lobe complex models (BFL) were based on a large dataset from Prélat (2010) collected within the medial to distal parts of Fan3. For the CLTZ-models two different datasets were used: one from Fan3 (OR) and one from Unit 5 (BK). The dashed outline represents the inferred outline of Fan 3.

Fig. 4. Panoramic views of the Fan 3 lobe complex at two locations at the Gemsbok Valley area. The level of lobe-on-lobe amalgamation is clearly different between both locations. Lobe numbers have been indicated; interlobes and interfan mudstones are presented in greyscale.

Fig. 5. (**A**) Panoramic view of central channelised area of the OR-section and its facies distribution based on log-data. Due to an exposure bias, the most dominant facies that can be observed is structureless sandstone. Red lines indicate erosion surfaces. (**B**) Typical channel-fill facies, with B1 –

mud clast conglomerates, both clast-supported (bottom) and matrix-supported (mid to top), B2– Soft-sediment deformed siltstones and sandstones at the channel margin, B3 – Structureless amalgamated sandstones and B4 – Banded argillaceous sandstones.

Fig. 6. *Left* - Log showing the Fan 3 basin-floor lobe complex and its division into six different lobes (based on Prélat *et al.* 2009). *Right* - Plan view of the simplified facies zones of four lobes used to construct the lobe complex facies models (based on Prélat 2010). All individual lobes show an irregular 'finger-like' facies distributions in frontal fringe areas.

Fig. 7. The two lobe construction models that have been applied with Lobe Model A: Stacking of all elements, creating a thickening/coarsening pattern at every single location of the lobe (based on Mutti 1977), and Model B: Facies transitions from axis to fringe (based on Prélat *et al.* 2009) with allowance of axial lobe amalgamation. The sketched fan in the middle shows the section (dashed white line) of the system (basin-floor lobe complex) that has been modelled. Different facies submodels were constructed for model B with a division into bottom, middle and top sections. B1: Simplified facies division with a single facies association for each lobe zone and no vertical division; B2: Multiple facies associations in top and bottom within off-axis areas and in fringe areas; and B3: Multiple facies associations within all lobe zones, including middle section of the off-axis areas.

Fig. 8. CLTZ reservoir block models with (**A**) OR submodels including a simplified (upscaled) facies distribution (OR-A) and a detailed (downscaled) facies distribution (OR-B); (**B**) BK submodels with two of the three having different levels of detail within channel-fills (BK Ch1 & BK Ch2) and one excluding the channels completely from the model (BK no-Ch). A full block-model of Bk Ch1 is shown as an example. Note that the facies proportion differences between the different submodels are limited.

Fig. 9. (**A**) Glitne Field core photos from well 15/5. Two core plug permeability measurements (A1 & A2) were undertaken within this sand-prone section (~5m), showing two completely different

permeability values, associated with a higher argillaceous content in A1, blocking pore space between individual grains. (**B**) Example of porosity range of the structureless sandstones (Fa1), determined based on the dataset of Bennes & Hamon (2007). Both permeability data from the Glitne field and grain size data from the outcrop record have been used to determine the range in porosity values. The shades of grey indicate the 'fine sands' group range for the associated permeability or grain size range.

Fig. 10. Table showing the range in porosity and permeability values applied within the petrophysical modelling, including core and outcrop examples. For certain facies groups (Fa2, F3 & Fa5) a permeability factor (Kv/Kh) was implemented to account for the expected heterogeneity within them.

Fig. 11. (**A**) Example porosity realisation of BFL-Model B2 showing stacked lobes and a decrease in porosity from axis to fringe. (**B**) Fence diagram of a horizontal permeability (Kh) realisation of BFL-Model B2, showing clear differences between axial and fringe facies. A total of 25 petrophysical property realisations were performed for every submodel.

Fig. 12. Well setup for BFL, OR and BK models. Injector and producer pairs were set at different locations with a fixed 1 km distance in between. Within the BFL-model two injector-producer pairs were located at different locations within the complex, an example of typical flow streamlines is shown on the right. Within the CLTZ models, the producer-injector pairs were orientated along channel orientation and positioned so that they penetrated the channel bodies. In the BK-model the wells penetrated the margins of both channel systems.

Fig. 13. Breakthrough time (TBT) histograms of all performed BFL model streamline simulations. The histograms show the results for the 25 simulations that were run for each well pair. Model A shows similar TBT's for different locations within the system, while Model B clearly shows differences

depending on location. The lower three histograms show the difference between the Model B submodels. The results of various two-tailed t-tests have been given to the right.

Fig. 14. Production curves showing difference in overall cumulative production between Model A and B and between locations within Model B2. The curves are composed from the (limited) spread resulting from a total of 5 different petrophysical realisations for each submodel.

Fig. 15. (A) Breakthrough time (TBT) histograms of all CLTZ models (OR & BK). Only limited differences can be observed between locations. A significant shift can be observed between the upscaled version (OR-A) and the downscaled version (OR-B). Streamlines in both models are all focused within the main channel facies (Fa1) as shown in the example below. The BK-model shows a similar shift in TBT from BK Ch1 to BK Ch2. Only a limited reduction (t-test results are given) is observed between BK Ch1 and BK no-Ch in breakthrough time. Production curves are not very different in all three cases, (based on 5 different simulations) but highest cumulative production is reached within the non-channelised model (BK no-Ch).**(B)** Summary table showing all the model alterations that have been studied and the average results from all performed streamline simulations and drainage functions.

Fig. 16. Summary conceptual model of macroscopic sweep efficiency versus tracer breakthrough time (TBT) within different lobe sub-environments. Different scenarios have been plotted and grouped into: non-amalgamated, amalgamated and channelised lobe areas. Both an early and late breakthrough will have negative consequences for sweep efficiency with a slow breakthrough indicating a badly connected injector-producer pair with low production rates and a very early breakthrough or a very well-connected injector-producer pair, but with significant loss of drainage area. Most uncertainty is associated with channelised lobe areas as heterogeneities can possibly cause compartmentalisation of the reservoir, while this does not occur within amalgamated lobe (HAZ) areas.

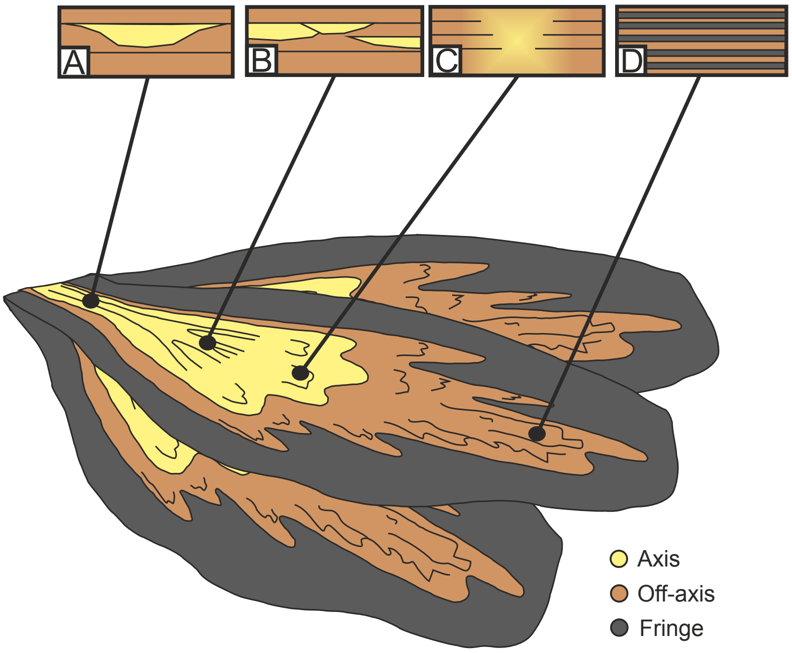
A
B
C
D
Axis
Off-axis
Fringe

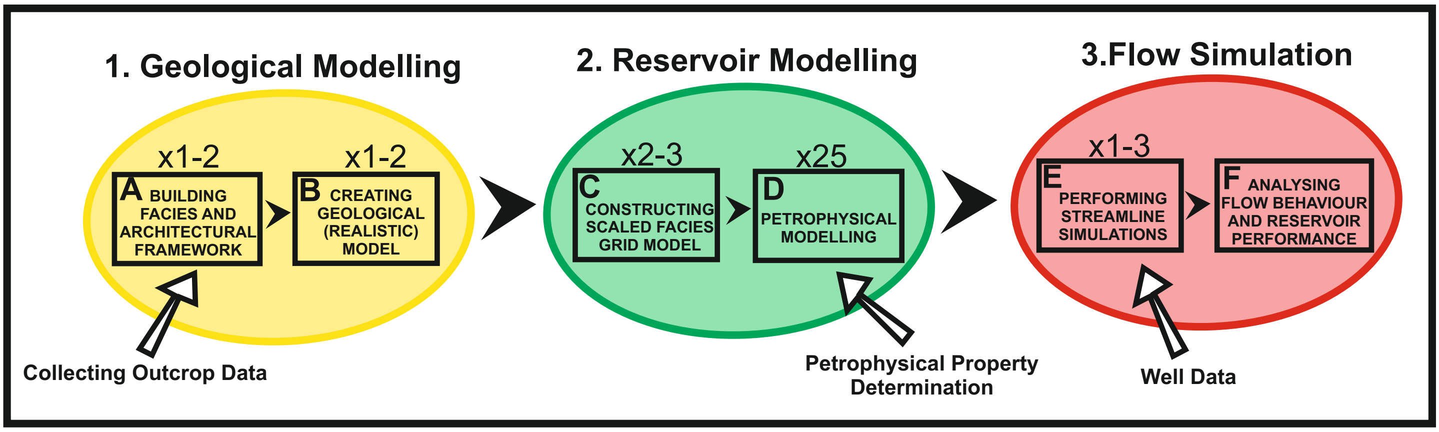

	Step	Active input	Main uncertainty	# Models	How uncertainty is covered/ reasons for multiple models
🟦	**A**	Outcrop data (Karoo Basin)	Correctness of sedimentary logs and correlations	CLTZ (2X) BFL (1X)	Different datasets modelled (CLTZ: BK & OR)
🟦	**B**	--	Interpretation of sedimentary architectures	CLTZ-OR (1X) CLTZ-BK (2X) BFL (2X)	Studying the effect of applying different models for lobe facies distributions (BFL: A & B) or the pressence/absence of channel-fills (BK: Ch & no-Ch)
🟦	**C**	--	Level of upscaling	BFL (3X) CLTZ-BK (2X) CLTZ-OR (2X)	Different levels of detail to look at the impact of fine-scale sedimentary architectures on connectivity
🟩	**D**	Petrophysical property data (Glitne Field)	Estimation of petrophysical properties linked to facies groups	25X	Stochastic modelling of petrophysical properties for each facies group - high number of realisations.
🟦	**E**	Well data (Glitne Field)	Well placement	Inj-Prod pairs BFL (2) OR(3) BK(1)	Different injector-producer pairs

🟦 Deterministic process 🟩 Stochastic process

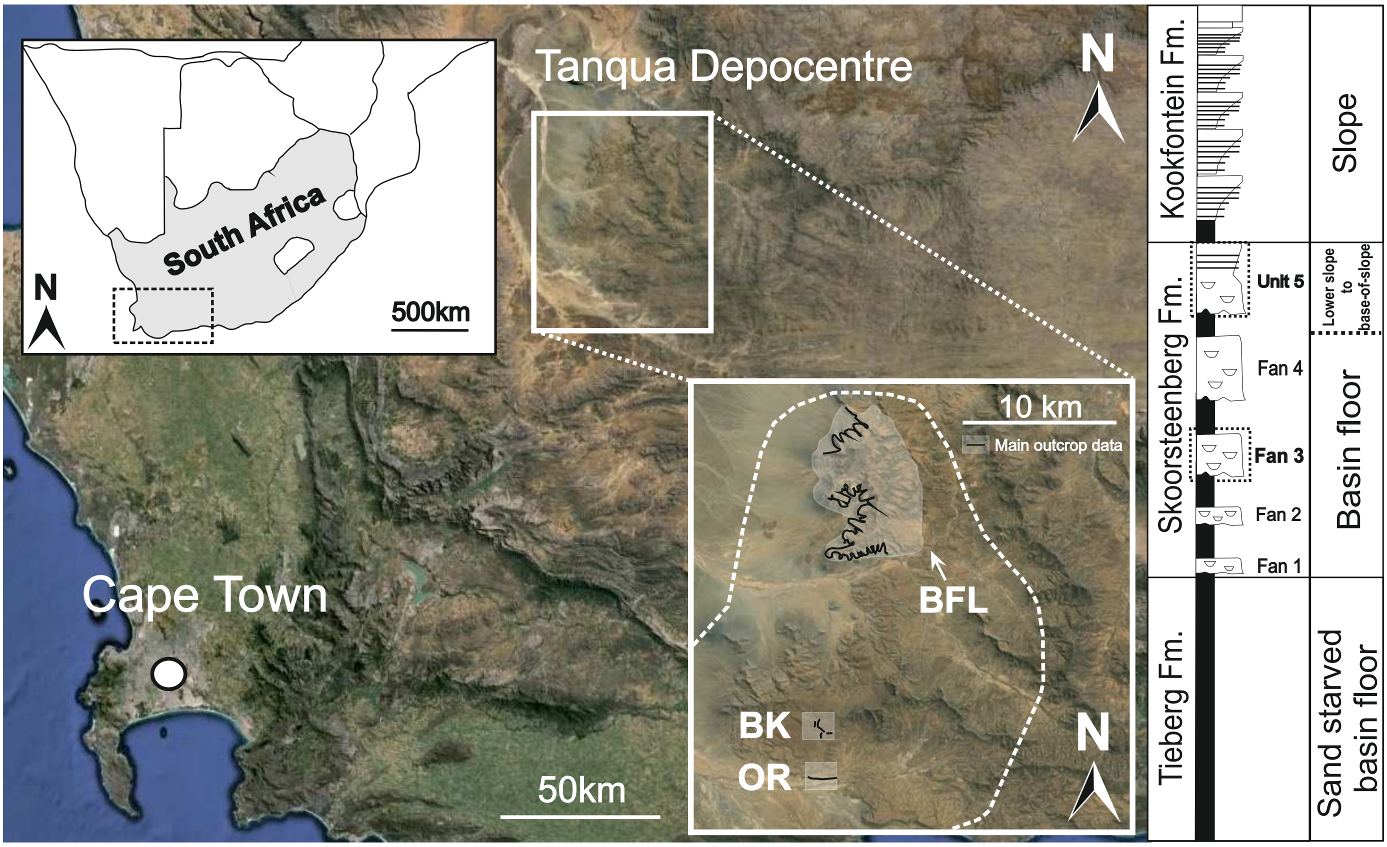
South Africa
N
500km
Tanqua Depocentre
N
Cape Town
50km
10 km
Main outcrop data
BFL
BK
OR
N
Kookfontein Fm.
Slope
Skoorsteenberg Fm.
Unit 5
Lower slope to base-of-slope
Fan 4
Fan 3
Fan 2
Fan 1
Basin floor
Tieberg Fm.
Sand starved basin floor

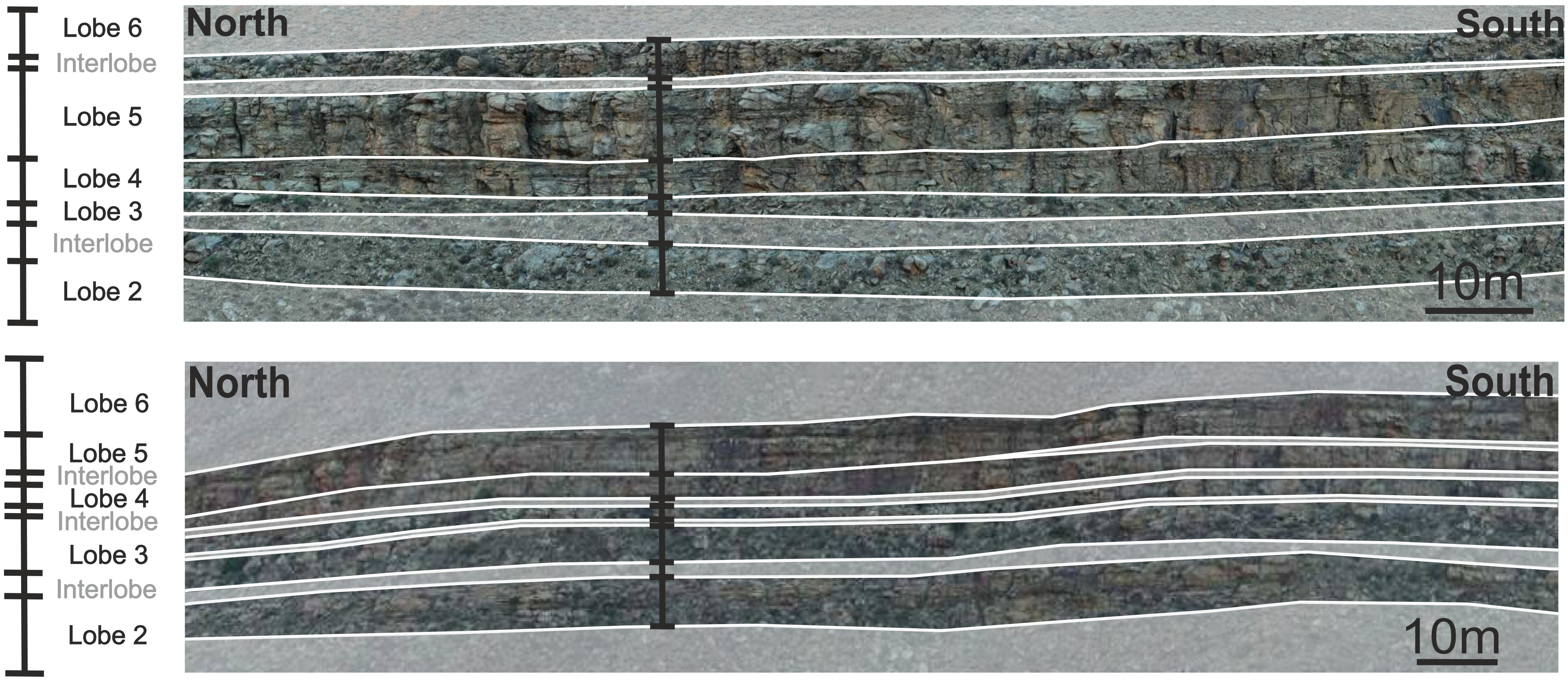
Lobe 6
Interlobe
Lobe 5
Lobe 4
Lobe 3
Interlobe
Lobe 2
North
South
10m
Lobe 6
Lobe 5
Interlobe
Lobe 4
Interlobe
Lobe 3
Interlobe
Lobe 2
North
South
10m

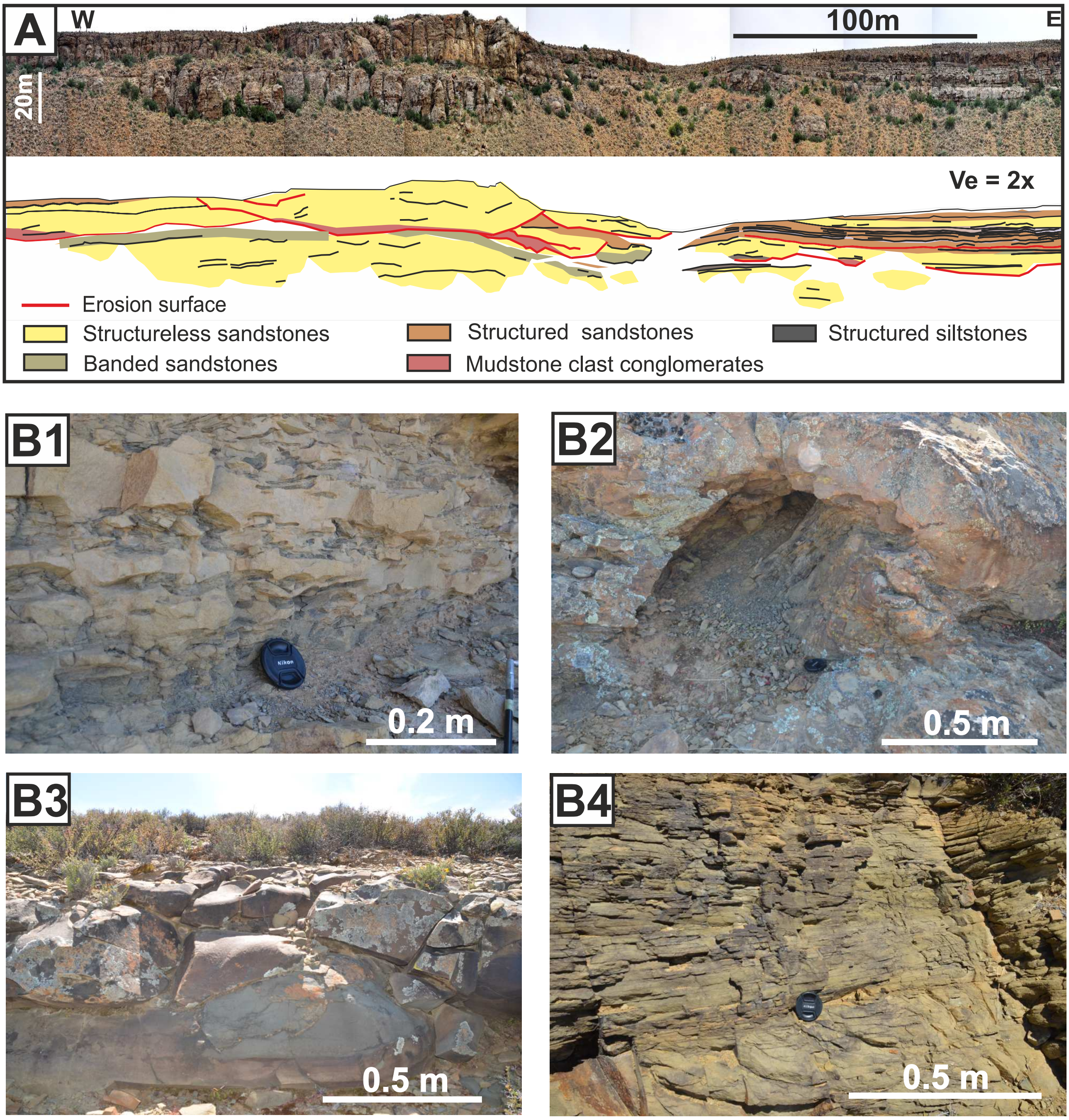
A
W
E
100m
20m
Ve = 2x
Erosion surface
Structureless sandstones
Banded sandstones
Structured sandstones
Mudstone clast conglomerates
Structured siltstones
B1
0.2 m
B2
0.5 m
B3
0.5 m
B4
0.5 m

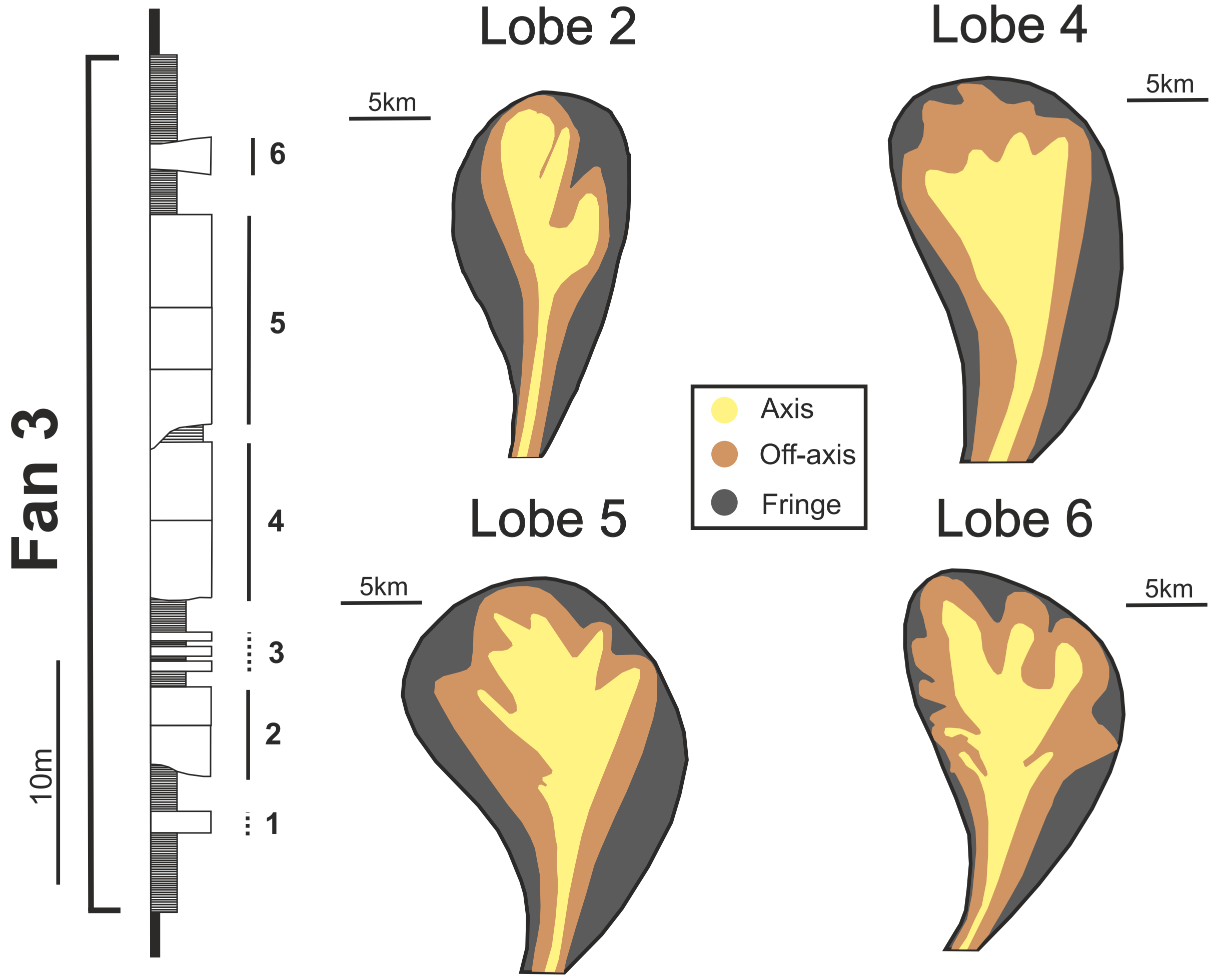
Fan 3
10m
6
5
4
3
2
1
Lobe 2
5km
Lobe 4
5km
Axis
Off-axis
Fringe
Lobe 5
5km
Lobe 6
5km

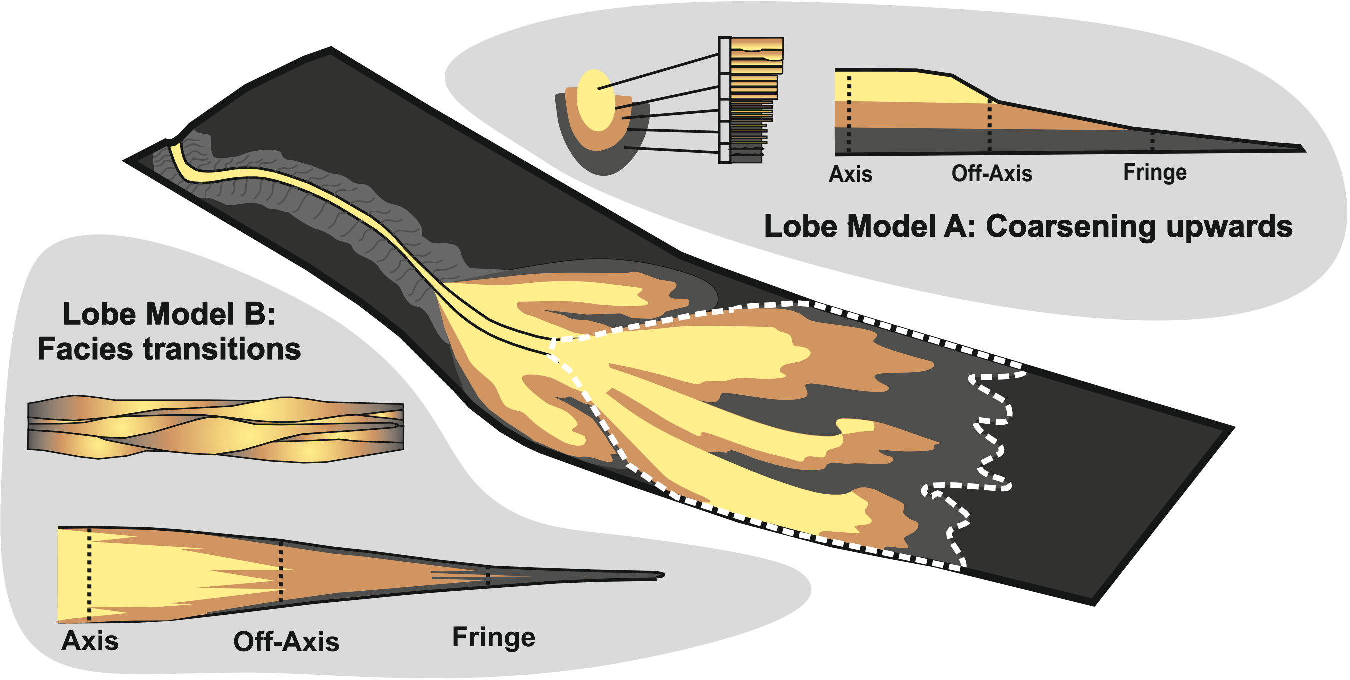

Cell size
x =100 m
y = 50 m
z = variable

🟨 **Structureless Sandstone**
🟧 **Structured Sandstone**
⬛ **Interbedded Sandstone and Siltstone**

		TR	Axis	Off-Axis	Fringe	
A	**Top**		33.3%	50%	100%	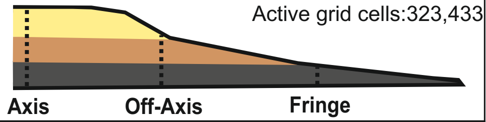 Active grid cells:323,433
	Middle		33.3%	50%		
	Bottom		33.3%			
B1 One facies for each zone	**Top**	0.25				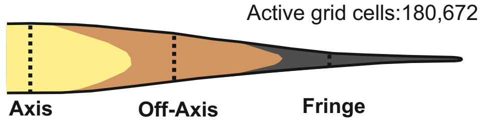 Active grid cells:180,672
	Middle	0.5	100%	100%	100%	
	Bottom	0.25				
B2 Multiple facies in off-axis to fringe	**Top**	0.25		50% 50%		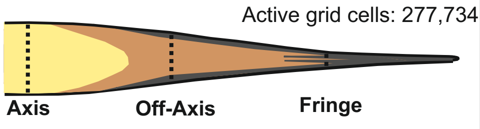 Active grid cells: 277,734
	Middle	0.5	100%	100%	25% 75%	
	Bottom	0.25		50% 50%		
B3 Multiple facies in each zone	**Top**	0.25	71.4% 28.6%	50% 50%		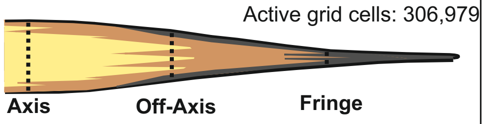 Active grid cells: 306,979
	Middle	0.5	100%	28.6% 71.4%	25% 75%	
	Bottom	0.25	71.4% 28.6%	50% 50%		

A

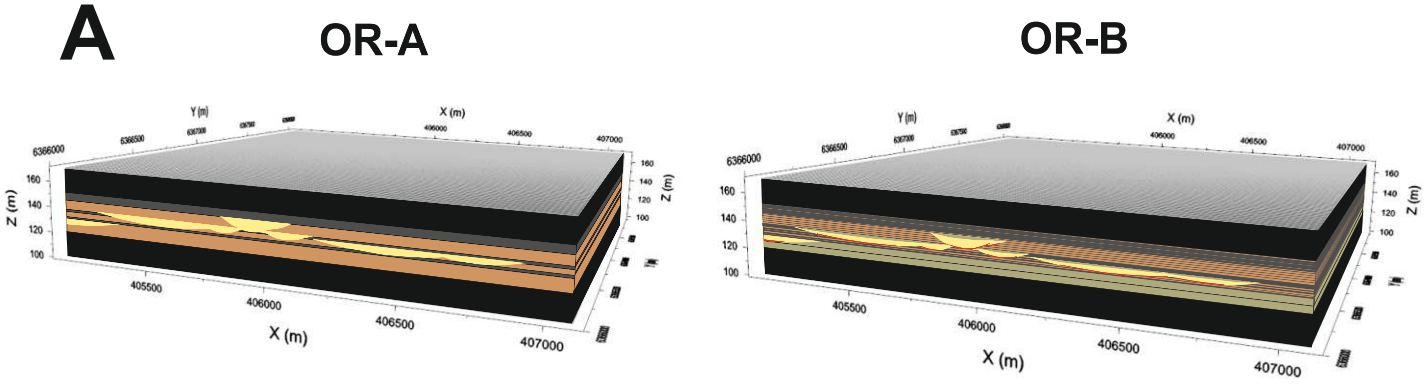

Model #	Characteristics	Facies Proportions	Active Grid Cells
OR-A	Upscaled *Non-detailed facies distribution*	31% 29% 27% 13%	69,195
OR-B	Downscaled *Detailed facies distribution*	27% 31% 31% 10% 1%	485,300

B

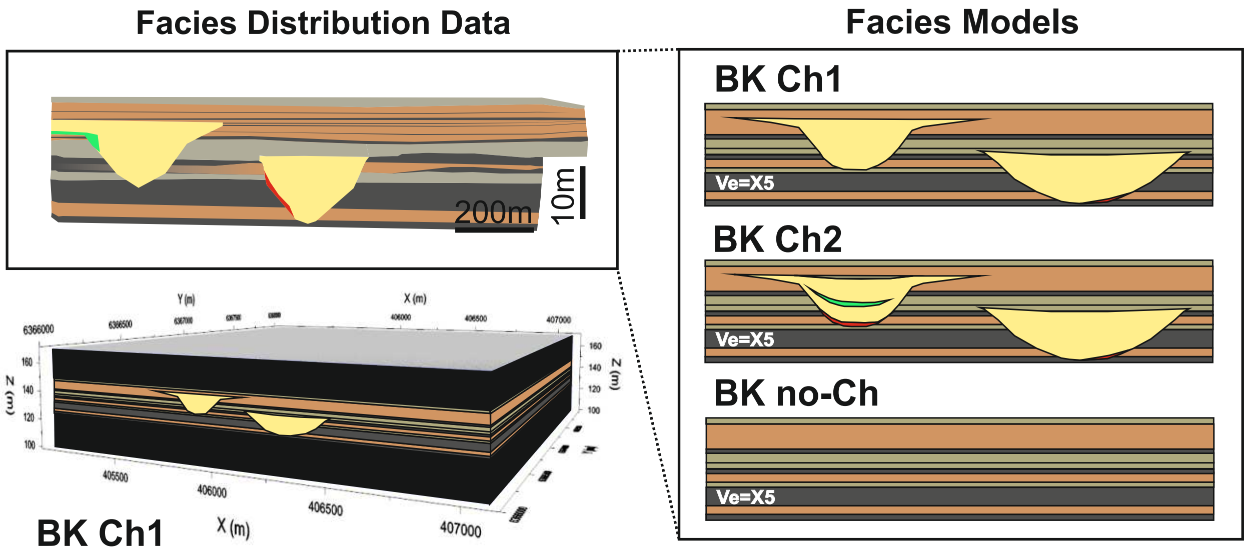

Model #	Characteristics	Facies Proportions	Active Grid Cells
BK Ch1	Channels (*uniform infill*)	38% 27% 24% 11%	121,651
BK Ch2	Channels (*complex infill*)	38% 27% 25% 9% 1%	150,282
BK no-Ch	Non-channelised	43% 31% 26%	107,811

🟧 Structured sandstones
⬛ Interbedded siltstones & sandstones
🟫 Structureless sandstones with argillaceous tops
🟨 Structureless sandstones
🟥 Mudstone clast conglomerates
🟩 Soft-sediment deformed deposits

A

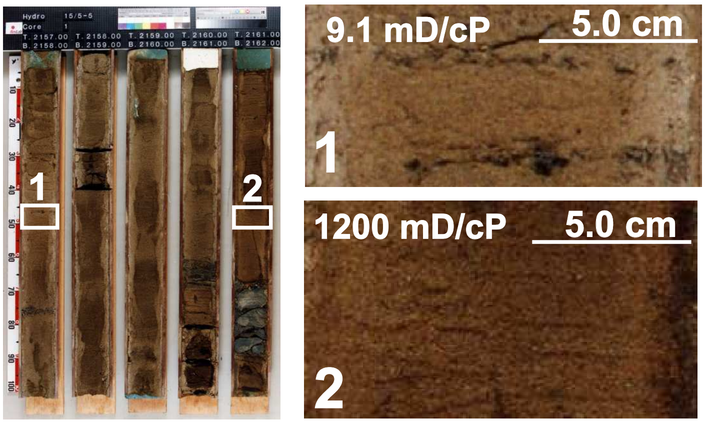
Hydro 15/5-5
Core 1
T. 2157.00 B. 2158.00
T. 2158.00 B. 2159.00
T. 2159.00 B. 2160.00
T. 2160.00 B. 2161.00
T. 2161.00 B. 2162.00
1
2
9.1 mD/cP
5.0 cm
1
1200 mD/cP
5.0 cm
2

B

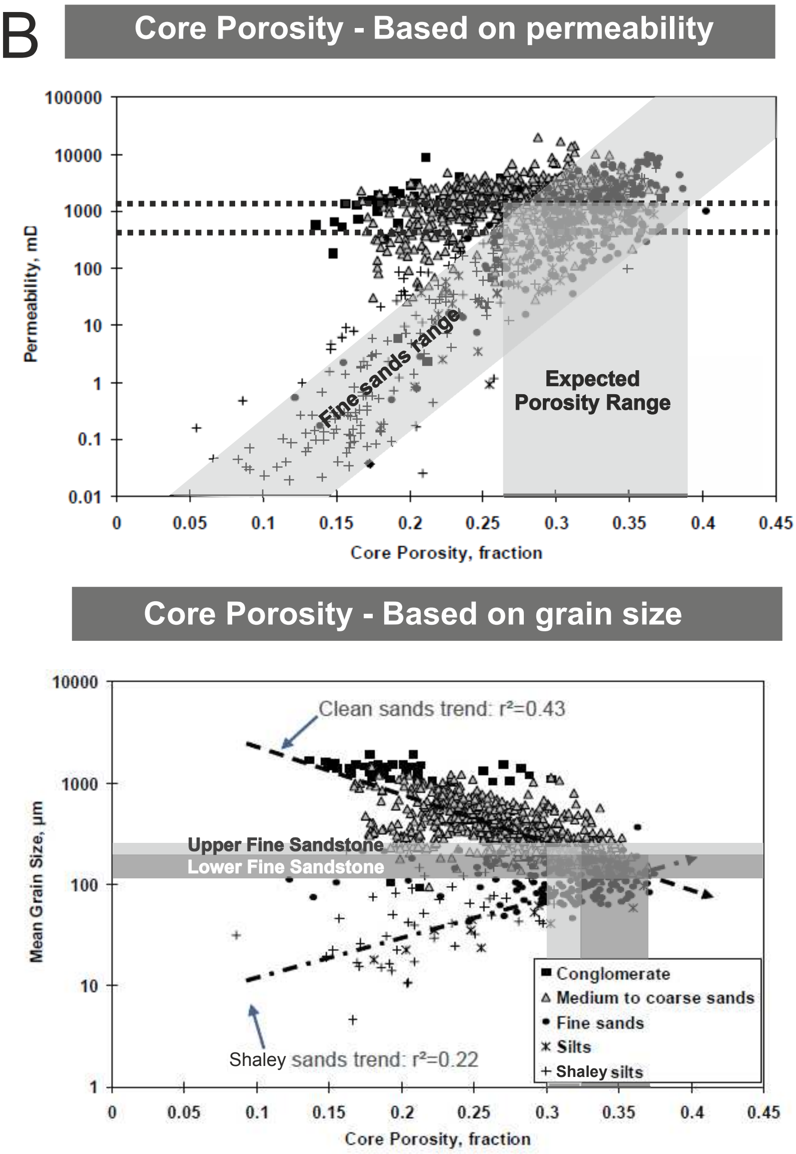
Core Porosity - Based on permeability
Permeability, mD
100000
10000
1000
100
10
1
0.1
0.01
0
0.05
0.1
0.15
0.2
0.25
0.3
0.35
0.4
0.45
Core Porosity, fraction
Fine sands range
Expected Porosity Range
Core Porosity - Based on grain size
Mean Grain Size, µm
10000
1000
100
10
1
Clean sands trend: r²=0.43
Upper Fine Sandstone
Lower Fine Sandstone
Shaley sands trend: r²=0.22
■ Conglomerate
△ Medium to coarse sands
● Fine sands
✱ Silts
+ Shaley silts
0
0.05
0.1
0.15
0.2
0.25
0.3
0.35
0.4
0.45
Core Porosity, fraction

	Fa 1A **Structureless Sandstone (AM)**	**Fa 1B** **Structureless Sandstone (TB)**	**Fa 2** **Structured Sandstones**	**Fa 3** **Siltstones & sandstones**	**Fa 4** **Mudclast Conglomerate**	**Fa 5** **Banded Sandstones**	**Fa 6** **SSD Deposits**
							
Porosity (fr)							
Mean	0.325	0.325	0.3	0.225	0.145	0.325	0.225
Range	0.26-0.39	0.26-0.39	0.23-0.36	0.16-0.29	0.09-0.20	0.26-0.39	0.16-0.29
Perm KH (mD)							
Mean	1200	800	220	60	2500	800	30
Range	600-1800	600-1200	150-300	1-100	10-5000	600-1200	0-60
Perm KV (mD)							
Mean	1200	800	110	15	2500	10	30
Range	600-1800	600-1200	75-150	1-25	10-5000	7.5-15	0-60
KV/KH	**1.0**	**1.0**	**0.5**	**0.25**	**1.0**	**0.0125**	**1.0**

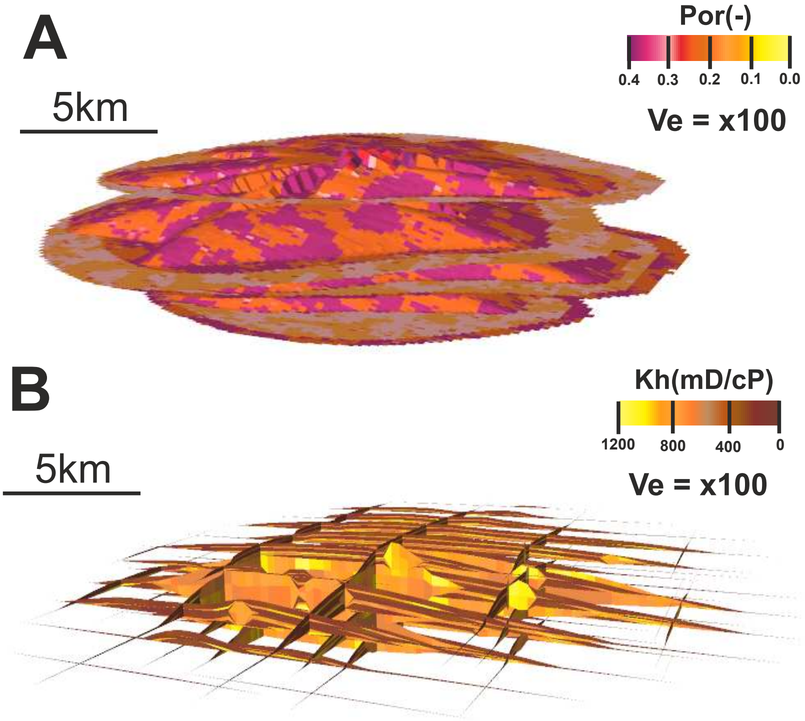
A
5km
Por(-)
0.4
0.3
0.2
0.1
0.0
Ve = x100
B
5km
Kh(mD/cP)
1200
800
400
0
Ve = x100

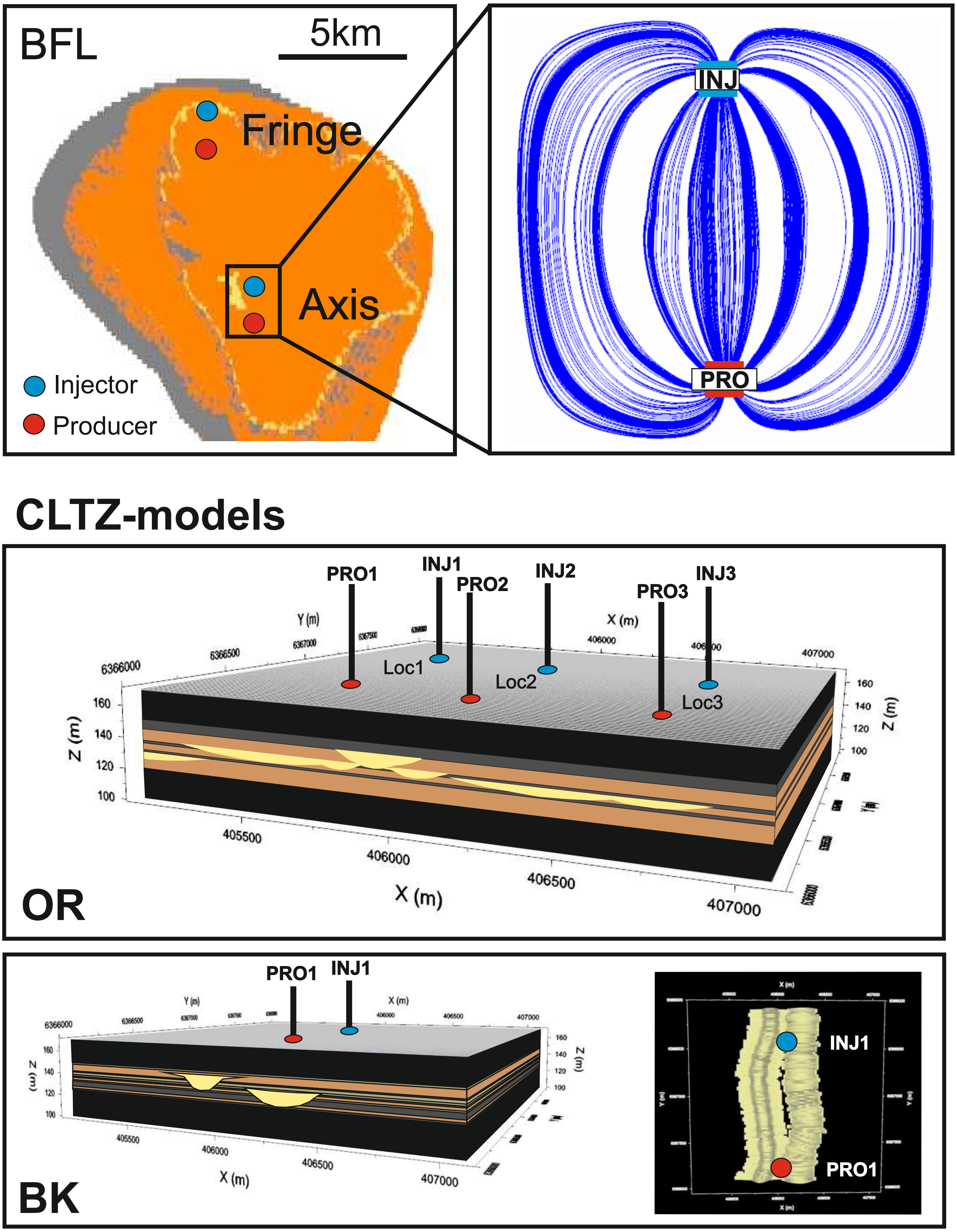
BFL
5km
Fringe
Axis
Injector
Producer
INJ
PRO
CLTZ-models
PRO1
INJ1
PRO2
INJ2
PRO3
INJ3
Loc1
Loc2
Loc3
Y (m)
X (m)
Z (m)
6366000
6366500
6367000
6367500
6368000
406000
406500
407000
160
140
120
100
405500
406000
406500
407000
X (m)
OR
PRO1
INJ1
BK
INJ1
PRO1
X (m)
Y (m)

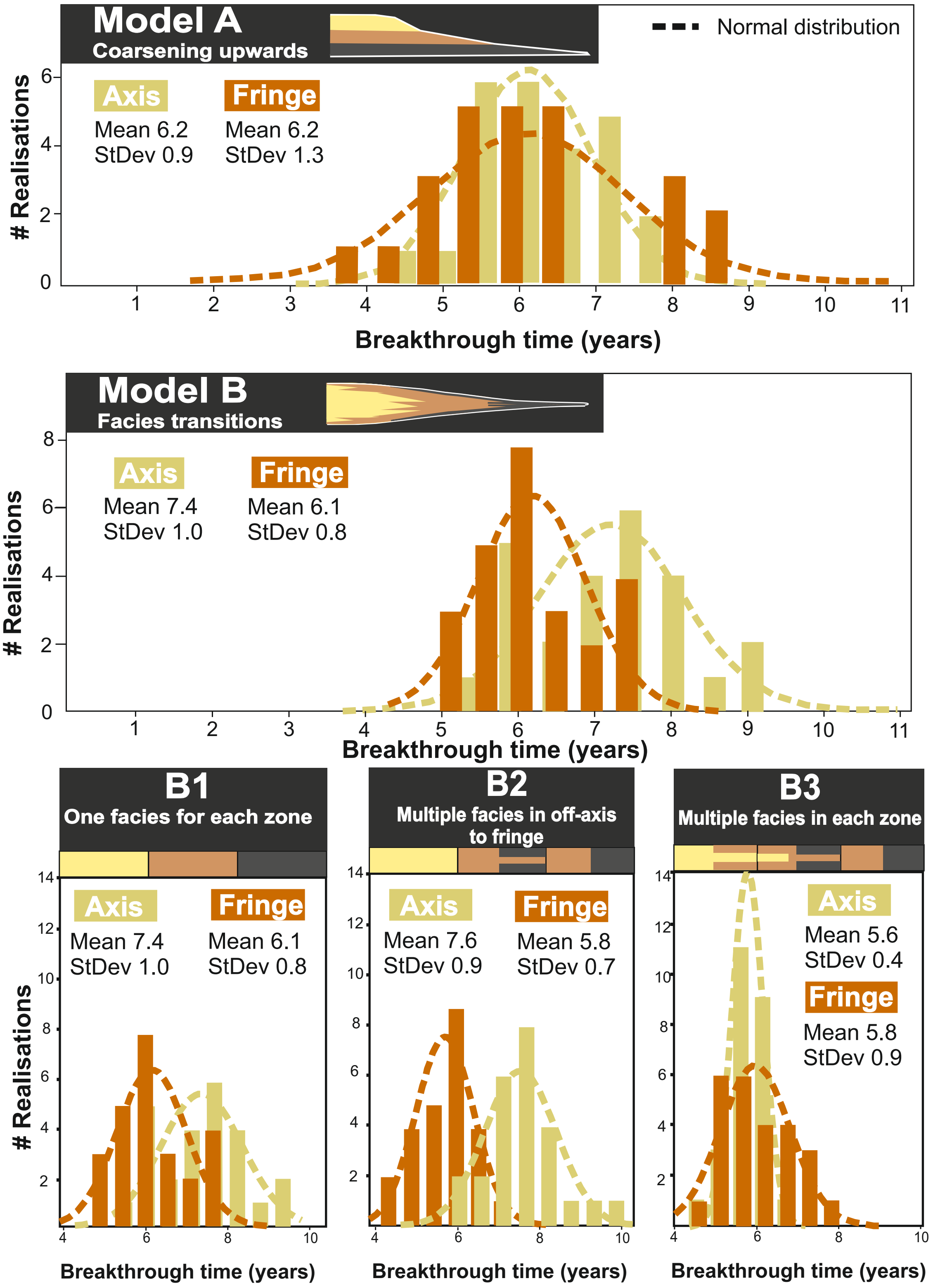

t-tests

Model A

H0: μ (Axis) = μ (Fringe)

t Stat	-0.072
P(T<=t) Two-tail	0.94
T Critical two-tail	2.02

Rejected? NO

Model B

H0: μ (Axis) = μ (Fringe)

t Stat	4.64
P(T<=t) Two-tail	2.78
T Critical two-tail	2.01

Rejected? YES

Model B1 & B2

H0: μ (Axis)B1 = μ (Fringe)B2

t Stat	-0.92
P(T<=t) Two-tail	0.36
T Critical two-tail	2.01

Rejected? NO

Model B1 & B2

H0: μ (Fringe)B1 = μ (Fringe)B2

t Stat	1.79
P(T<=t) Two-tail	0.08
T Critical two-tail	2.01

Rejected? NO

Model B1 & B3

H0: μ (Axis)B1 = μ (Axis)B3

t Stat	8.05
P(T<=t) Two-tail	4.30
T Critical two-tail	2.04

Rejected? YES

Model B1 & B3

H0: μ (Axis)B1 = μ (Axis)B3

t Stat	1.39
P(T<=t) Two-tail	0.17
T Critical two-tail	2.01

Rejected? NO

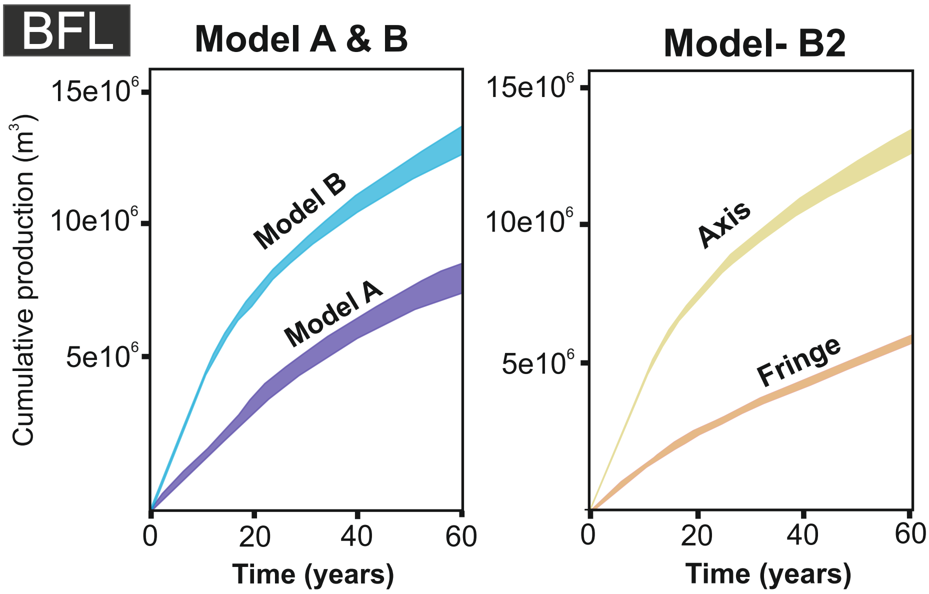
BFL
Model A & B
Model- B2
Cumulative production (m³)
15e10⁶
10e10⁶
5e10⁶
Model B
Model A
Axis
Fringe
0
20
40
60
Time (years)

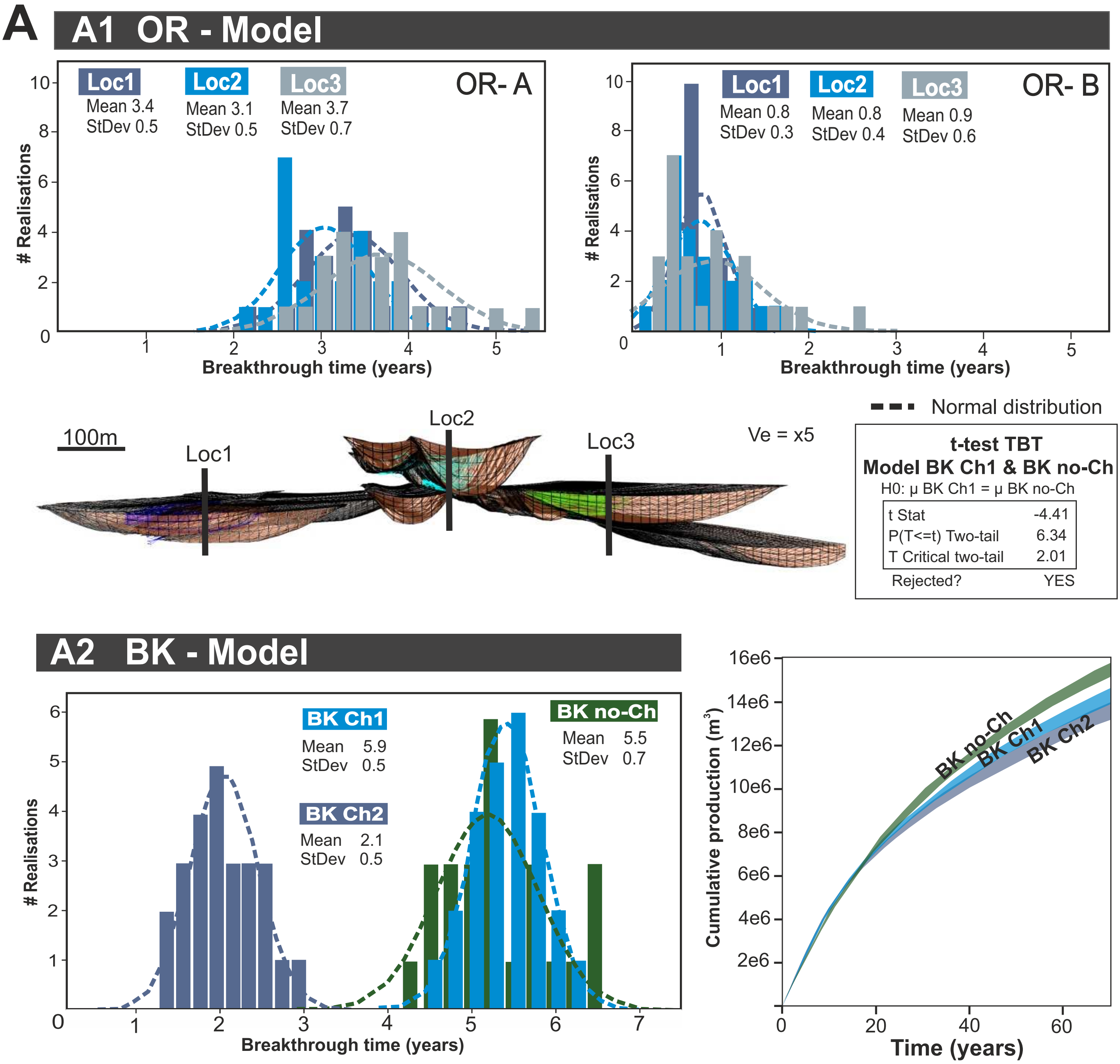

B

Models compared	Effect studied	Impact TBT	C prod
LOBES			
A ➤ B	applying facies transitions instead of coarsening upward structures in lobes	A: +~20% F: NSI	+~40% (40yrs)
B1 ➤ B2	applying facies alterations in non-axis areas of lobes	A: NSI F: NSI	(A +~60% relative to F)
B1/B2 ➤ B3	applying facies alterations in all lobe areas	A: +~30% F: NSI	
CLTZ			
OR1 ➤ OR2	Downscaling of the full model	~-75%	
BK Ch1 ➤ BK Ch2	Applying heterogeneities in channel-fills	~-65%	~-3% (40yrs)
BK Ch1 ➤ BK no-Ch	Removing channels from the model	NSI	~-8% (40yrs)

🟩 Increase 🟧 Constant 🟥 Decrease

A = Axis; F = Fringe; NSI = No significant impact; TBT = Tracer breakthrough time; C prod = Cummulative production

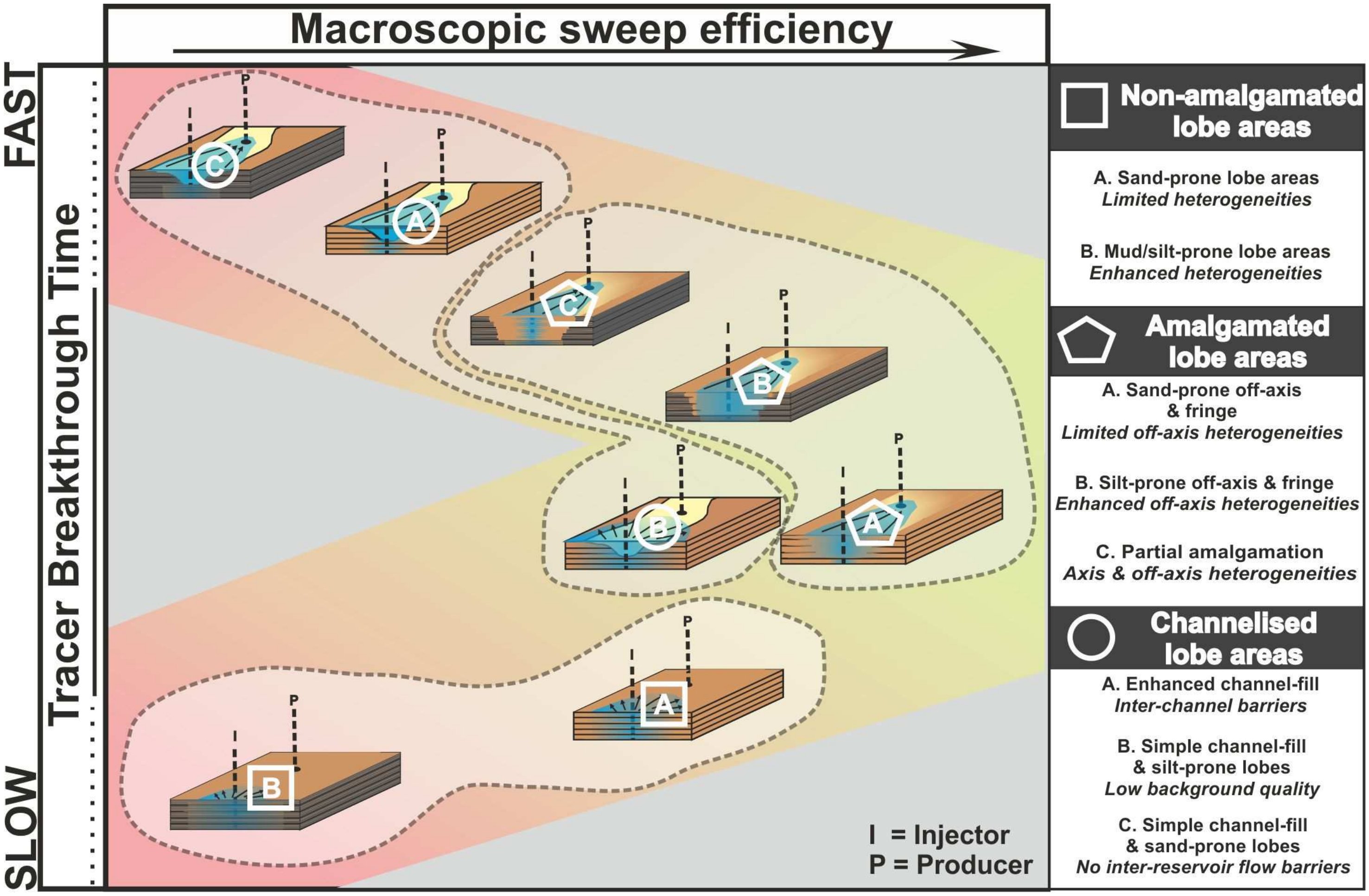
Macroscopic sweep efficiency
FAST
Tracer Breakthrough Time
SLOW
P
I
C
A
B
I = Injector
P = Producer
□ Non-amalgamated lobe areas
A. Sand-prone lobe areas
Limited heterogeneities
B. Mud/silt-prone lobe areas
Enhanced heterogeneities
⬠ Amalgamated lobe areas
A. Sand-prone off-axis & fringe
Limited off-axis heterogeneities
B. Silt-prone off-axis & fringe
Enhanced off-axis heterogeneities
C. Partial amalgamation
Axis & off-axis heterogeneities
○ Channelised lobe areas
A. Enhanced channel-fill
Inter-channel barriers
B. Simple channel-fill & silt-prone lobes
Low background quality
C. Simple channel-fill & sand-prone lobes
No inter-reservoir flow barriers